UNIVERSITY OF THESSALY

SCHOOL of ENGINEERING

DEPARTMENT OF MECHANICAL ENGINEERING

Preliminary design of a Knudsen pump

by

Aristea Maniou

Mechanical Engineer

University of Thessaly, 2011

A Master's Thesis Submitted for the Partial Fulfillment of the Requirements for the Degree of

MASTER OF SCIENCE

Volos 2011

Certified by the members of the Dissertation Committee:

1st member: Dr. Valougeorgis D.
(Supervisor) Professor, Department of Mechanical Engineering
University of Thessaly

2nd member: Dr. Andritsos N.
Associate Professor, Department of Mechanical Engineering
University of Thessaly

3rd member: Dr. Grammenos Th.
Lecturer, Department of Civil Engineering
University of Thessaly

Dedicated to my family

Acknowledgements

First and foremost, I would like to express my gratitude to my supervisor Professor Dimitris Valougeorgis for teaching and supporting me during my M. Sc. Without his constant support and mentorship, this dissertation would not have been completed. His patience and guidance, provided throughout the course of our cooperation, are the two key factors that contributed to the completion of my M. Sc. thesis.

I am also grateful to the other two members of the Committee, Professors Andritsos Nikolaos and Grammenos Theophanes, for their careful reading of my dissertation and their valuable suggestions.

In the writing of my thesis, Misdanitis Serafeim, Dr. Steryios Naris and Dr. Sarantis Pantazis also contributed, and I must thank them as well for, their assistance throughout my graduate work has really been invaluable.

Finally, and above all, I am grateful to my parents for their support and encouragement during all these years.

Volos, September 2011

Aristea Maniou

PRELIMINARY DESIGN OF A KNUDSEN PUMP

ARISTEA MANIOU

University of Thessaly, Department of Mechanical Engineering, 2011

Supervisor: Dr. D. Valougeorgis, Professor, Mesoscale Methods in Flows and Transport Phenomena

Abstract

In this work, the phenomenon of thermal transpiration, also referred to as "thermal creep", is studied. The Knudsen pump, is a type of vacuum pump that works by the principle of thermal transpiration. First of all, the dimensionless Knudsen number is defined, and the flow regimes, according to the different Knudsen numbers, are mentioned. A simple description of the phenomenon of thermal transpiration is provided.

The purpose of this work is to investigate the basic flow configuration related to a preliminary design of a Knudsen pump, and for this we apply kinetic model equations to investigate the rarefied gas flow through a cylindrical tube whose ends are maintained at different temperatures.

A detailed literature review of the phenomenon is provided along with details concerning the kinetic models developed to approximate the problem. The description of the problem and the formulation of the corresponding kinetic equations are presented, as well as the simulation of the boundary conditions. The problem is described by the integro – differential Boltzmann equation, which is used to determine the distribution of particles in physical and molecular velocity space, as well as in time. The macroscopic quantities of practical interest are obtained from the moments of the distribution function.

The kinetic model used in the simulations was the ellipsoidal model. In particular, we apply the non – linear ES model subject to Maxwell diffuse boundary conditions, to solve the non – isothermal flow of a rarefied gas through a cylindrical tube. The solutions provided, are valid in the whole range of the Knudsen number.

Results regarding the flow, for the bulk quantities of velocity, heat flux, temperature and density are presented in terms of the three dimensionless parameters describing the flow, namely the rarefaction parameter δ, the temperature ratio T_{in}/T_{out} and the channel aspect ratio L/R.

Finally, an overview of this work is presented together with some concluding remarks and some suggestions concerning future work in this field.

ΠΡΟΚΑΤΑΡΚΤΙΚΗ ΜΕΛΕΤΗ ΤΗΣ ΑΝΤΛΙΑΣ KNUDSEN

ΑΡΙΣΤΕΑ ΜΑΝΙΟΥ

Πανεπιστήμιο Θεσσαλίας, Τμήμα Μηχανολόγων Μηχανικών, 2011

Επιβλέπων Καθηγητής: Δρ. Δημήτριος Βαλουγεώργης, Καθηγητής Αναλυτικών και Υπολογιστικών Μεθόδων Μεσοκλίμακας σε Φαινόμενα Ροής και Μεταφοράς

Περίληψη

Στην παρούσα μεταπτυχιακή εργασία μελετάται το φαινόμενο του θερμικού ερπυσμού, στο οποίο βασίζεται και η λειτουργία της αντλίας Knudsen. Αρχικά, γίνεται μια γενική αναφορά στα φαινόμενα ροής και μεταφοράς εκτός θερμοδυναμικής ισορροπίας και ορίζεται ο αδιάστατος αριθμός Knudsen. Παρουσιάζονται οι περιοχές της ροής , όπως αυτές διακρίνονται με βάση τον αριθμό Knudsen, καθώς επίσης και κάποια στοιχεία που αφορούν στις μεθοδολογίες επίλυσης. Δίνεται μια συνοπτική περιγραφή του φαινομένου του θερμικού ερπυσμού (thermal creep) και μια αναφορά σε πιθανές εφαρμογές, συμπεριλαμβανόμενης της αντλίας Knudsen.

Σκοπός της εργασίας είναι η προκαταρκτική μελέτη της αντλίας Knudsen, επιλύοντας το πρόβλημα ροής σε κυλινδρικό αγωγό λόγω διαφοράς θερμοκρασίας, ώστε να προκύψουν ποσοτικά αποτελέσματα σχετικά με τη ροή, που θα μας επιτρέψουν να εκτιμήσουμε τα χαρακτηριστικά και τις ιδιαιτερότητές της. Έτσι θα μπορέσουν να προκύψουν τα πρώτα συμπεράσματα σχετικά με το σχεδιασμό και τις πραγματικές δυνατότητες της αντλίας Knudsen.

Ακολούθως, παρουσιάζεται λεπτομερής βιβλιογραφική ανασκόπηση του φαινομένου του θερμικού ερπυσμού, συμπεριλαμβανομένων των ροών σε αγωγούς μεγάλου μήκους όπου η ροή θεωρείται πλήρως ανεπτυγμένη αλλά και των ροών σε αγωγούς πεπερασμένου μήκους.

Έπεται η διατύπωση του προβλήματος. Δίνεται η περιγραφή της γεωμετρίας που μελετήθηκε, παρουσιάζονται οι κινητικές εξισώσεις και διατυπώνονται οι συνοριακές συνθήκες. Στην προσέγγιση με βάση την κινητική θεωρία, όπως αυτή εκφράζεται μέσω της εξίσωσης Boltzmann, ο βασικό άγνωστος είναι η συνάρτηση κατανομής, ενώ οι μακροσκοπικές ποσότητες που μας ενδιαφέρουν προκύπτουν από τις ροπές της συνάρτησης κατανομής.

Τα κινητικά μοντέλα, σε αρκετές εφαρμογές έχουν αποδειχθεί αρκετά αξιόπιστα, και χρησιμοποιούνται εναλλακτικά αντί της εξίσωσης Boltzmann, δίνοντας ακριβή αποτελέσματα σε όλο το εύρος του αριθμού Knudsen. Το κινητικό μοντέλο που χρησιμοποιήθηκε είναι το ελλειψοειδές μοντέλο (ellipsoidal model, ES) για μη ισοθερμοκρασιακές ροές. Παρουσιάζεται η αριθμητική μέθοδος για ροή σε αγωγούς πεπερασμένου μήκους και αναφέρονται οι ιδιαιτερότητες του αλγορίθμου, στην περίπτωση του θερμικού ερπυσμού.

Στη συνέχεια, παρουσιάζονται τα αποτελέσματα που προκύπτουν, τα οποία βρίσκονται συγκεντρωμένα σε πίνακες, στο τέλος του αντίστοιχου κεφαλαίου.

Τέλος, γίνεται μια σύνοψη όλων των παραπάνω, καταγράφονται τα συμπεράσματα που προέκυψαν από την παρούσα εργασία, και προτείνονται θέματα που μπορούν να μελετηθούν ως συνέχεια της εργασίας αυτής.

TABLE OF CONTENTS

Chapter 1

Introduction

1.1 General concepts

Manufacturing processes that can create extremely small machines have been developed in recent years. Electrostatic, magnetic, electromagnetic, pneumatic and thermal actuators, motors, valves, gears, cantilevers, diaphragms and tweezers less than 100 μm in size have been fabricated. These have been used as sensors for pressure, temperature, mass flow, velocity, sound and chemical composition; as actuators for linear and angular motions; and as simple components for complex systems such as robots, micro-heat-engines and micro-heat-pumps.

Microelectromechanical systems (MEMS) refer to devices that have a characteristic length of less than 1 mm but more than 1 μm, that combine electrical and mechanical components and that are fabricated using integrated circuit batch-processing technologies [Gad – el – Hak, 2002].

In this wide variety of applications, encountered in our everyday life, gas flows are very important. The development of such devices, as the ones mentioned above, has opened up an entirely new field of research where the behaviour of flows far from equilibrium conditions is very important.

In most cases, the equations of mass, momentum and energy equilibrium combined by the Newton – Fourier – Fick constitutive equations, describe their behaviour very well and have been actually applied successfully for many years. However, this formulation is subject to certain limitations due to the underlying assumption that the gas must be considered as a continuum medium. Even though this is a reasonable assumption for many cases, there are situations where this hypothesis fails, as the mean free path between inter - molecular collisions may become comparable to a characteristic length, due to conditions of low pressure or if the gas is confined in a region of very small dimensions. In such cases the continuum medium assumption collapses [Misdanitis, 2009].

Beyond a certain limit, it is not possible to investigate such phenomena accurately without taking into account the molecular nature of the gas. In this case, we

may say that the gas is in a rarefied state, for which the departure from the thermodynamic equilibrium leads to a failure of the macroscopic equations. To deal with these cases, several approaches are used depending on the application under study. Concepts derived from statistical mechanics and the kinetic theory of gases, need to be involved.

The governing equation is the Boltzmann equation, which is based on the kinetic theory of gases used to describe transport phenomena, with emphasis on dilute gas systems. This equation concerns the distribution function of particles, a 7-dimensional probability density distribution of molecules in the physical space, molecular velocity space and time. Like all methods, the statistical approach through the Boltzmann equation is characterized by its respective advantages and disadvantages The Botzmann equation is quite complex and can be solved analytically only for very specific situations, a fact that often leads us to the pursuit of numerical solutions, since the experimental investigation is, usually, very costly. However, the solution of this equation, though painful, is widely used today and leads to a good approach for a large number of problems with satisfactory results.

Rarefied gas flows are mainly found in small devices and low-pressure applications. The characteristic number that determines the degree of rarefaction and the area in which continuum model equations are valid is the Knudsen number (Kn), which is defined by the relationship

$$Kn = \frac{\lambda}{L} = \sqrt{\frac{\gamma\pi}{2}} \frac{Ma}{Re} \qquad (1.1)$$

where L is a characteristic dimension of the problem, λ the mean free path of the particles, γ the ratio of specific heats, Ma the Mach number and Re the Reynolds number. The mean free path is defined as the average distance travelled by molecules between collisions and can be mathematically expressed by multiplying the average molecular velocity $\bar{\xi}$ to the mean free time, i.e.

$$\lambda = \bar{\xi}\tau \qquad (1.2)$$

The average molecular velocity is given by

$$\bar{\xi} = \sqrt{\frac{3k_B T}{m}} = \sqrt{3RT}\,. \qquad (1.3)$$

where k_B is the Boltzmann constant $\left(k_B = 1.3805 \times 10^{-23} J/K\right)$, m the molecular mass and R the specific gas constant. If ν is the collision frequency, which is determined by dividing the number of collisions N that occur in the time unit to the total number of molecules n in a unit volume, then the mean free time between collisions equals

$$\tau = \frac{1}{\nu} = \frac{n}{\mathrm{N}} \qquad (1.4)$$

The mean free path cannot be measured directly and may be calculated on the basis of measured macroscopic quantities in accordance to the relationship [Sharipov & Seleznev, 1998]

$$\lambda = \frac{\sqrt{\pi}\mu}{2P}\upsilon_0 \qquad (1.5)$$

where P is the local pressure, μ the dynamic viscosity at local temperature T, and

$$\upsilon_0 = \sqrt{\frac{2k_B T}{m}} = \sqrt{2RT}\,. \qquad (1.6)$$

υ_0 is the most probable molecular velocity. The quantity υ_0 is often used to non-dimensionalise the molecular velocity. It must also be noted here, that, the relationship (1.5) is valid for the hard sphere model (HS), in which the molecules are pictured as impenetrable billiard balls of specific diameter. Another molecular velocity of some interest is the mean thermal velocity

$$\langle \upsilon \rangle = \frac{2}{\sqrt{\pi}}\upsilon_0 \qquad (1.7)$$

Also, the gas rarefaction parameter δ is frequently used, which is linked to the Knudsen number as follows [Sharipov & Seleznev, 1998]:

$$\delta \equiv \frac{\sqrt{\pi}}{2}\frac{L}{\lambda} = \frac{\sqrt{\pi}}{2}\frac{1}{Kn} = \frac{LP}{\mu}\sqrt{\frac{m}{2k_B T}} = \frac{LP}{\mu \upsilon_0} \qquad (1.8)$$

The Kn number (or rarefaction parameter δ) is characteristic of any problem (e.g. study of heat transfer effects through rarefied gases, study of non – linear flows driven by large pressure differences for small length ratios) and its value characterizes the flow of gas. The local value of the Knudsen number in a particular flow determines the degree of rarefaction and the degree of validity of the continuum model. The different Knudsen number regimes are determined empirically and they are, therefore, only approximate for a particular flow geometry and they have been specified in the pioneering experiments conducted by Knudsen in 1909. In the limit of a zero Knudsen number, the mean free path is zero, i.e. for $P \neq 0$ the viscosity is zero and then the Navier–Stokes equations reduce to the inviscid Euler equations. The equivalent molecular viewpoint is described by the local Maxwellian distribution. As Kn increases, rarefaction effects become more important and, eventually, the Navier–Stokes equations break down. The different Knudsen number regimes are depicted in Figure 1.1 and can be summarized as follows:

- $Kn = 0, (\delta \to \infty)$: **Hydrodynamic Limit.** Here the Euler equations are valid.
- $Kn < 10^{-3}$ $(\delta > 10^{3})$: **Hydrodynamic Regime.** The gas may be considered as a continuum medium and the Navier – Stokes equations are applicable, coupled with no-slip boundary conditions.
- $10^{-3} \le Kn < 10^{-1} (10^{3} \le \delta \le 10)$: **Slip regime.** Non – equilibrium phenomena start manifesting in the boundary regions of the domain. In particular, velocity slip and temperature jump are observed on the walls.
- $10^{-1} < Kn < 10 (10 > \delta > 10^{-1})$: **Transition regime.** A kinetic description of the gas is necessary, since intermolecular collisions are reduced and the distribution function is not of the Maxwellian type. The Boltzmann equation is

valid here. It is noted that the validity of the Boltzmann equation is extended well outside the transition regime.

- $Kn > 10 (\delta < 10^{-1})$: **Free molecular regime.** The molecules undergo ballistic motion and remain unaffected by other molecules. No intermolecular collisions take place in this regime.

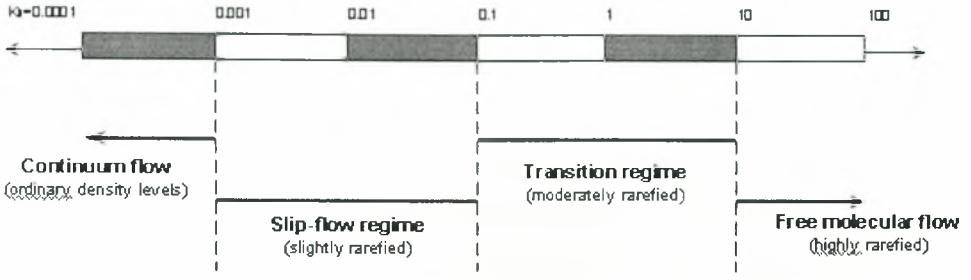

Figure1.1: Knudsen number regimes (Gad-el-Hak, 2002)

As we depart from the hydrodynamic regime, non – equilibrium phenomena appear: The gas and the wall surface do not have the same velocity, or temperature, secondary flows are induced by temperature gradients (or concentration gradients for mixtures) and so on. These phenomena cannot be captured by the classical hydrodynamic equations and can be examined via the kinetic theory of gases. The problem is described by the integro-differential Boltzmann equation, which is used to determine the distribution of particles in physical and molecular velocity space, as well as in time. There are difficulties associated with the seven-dimensional nature of the distribution function, as well as with the complexity of the collision term, which is usually substituted by an appropriate model.

1.2 Thermal Transpiration flow

Thermal transpiration flow is the macroscopic movement of a rarefied gas, induced by a temperature gradient. It is well known that by applying a disequilibrium of temperature to a tube filled with a rarefied gas, without any initial difference of pressure or any difference in chemical constitution, the gas will macroscopically

move from the lower to the higher temperature zone. This phenomenon was named by Reynolds *Thermal Transpiration*, in 1878. Reynolds [Reynolds, 1879], in an investigation with a plaster-of-Paris plug separating two regions, one cold region and one hot region, maintained at different temperatures T_C and T_H, showed that at very low densities, the equilibrium pressures on the two sides are related by the law

$$\frac{p_H}{p_C} = \left(\frac{T_H}{T_C}\right)^{1/2} \quad (1.9)$$

Maxwell closely followed this investigation up by mathematically analyzing the phenomenon using the, at the time, still controversial kinetic theory. Later on, in 1909, Knudsen proved Reynolds's law for the case of a tube by using both theoretical and experimental research [Cardenas et al., 2011]. In the experiment presented by Knudsen, two pressure gauges are joined by a pipe with several narrow and wide sections, where every second joint of the sections of the pipe is heated, in order for the temperature of the heated and unheated joints to be kept at 500°C [Sone et al., 1996]. Knudsen's research led to the supposition that the above cited law was valid only at a zero-flow final equilibrium state, which followed a transitional stage of gas displacement [Cardenas et al., 2011]. Since then, various researchers have contributed intermittently towards the understanding of thermal transpiration flow [Gupta et al., 2007].

A simple experiment to demonstrate a rarefied gas flow induced along an unequally heated wall was proposed by Y. Sone [Sone, 1991]. The experimental apparatus, which is shown in Fig. 1.2, consists of a rectangular glass plate, which is set with its longer sides in the vertical direction, and an electric heater on Nichrome wire is placed near the lower side of the back of the plate. A windmill to detect vertical wind is placed in front of the plate. The whole system is placed in a cylindrical vacuum chamber of a glass bell jar on a steel base, where the pressure can be controlled between atmospheric condition and several Pascals. The cellophane vanes of the windmill are suspended on a needle and rotate by vertical wind. When heated, the temperature of the plate is about 34°C near its upper side, 50°C in the middle, 63°C at the height of the vanes and 140°C at the lower side of the plate.

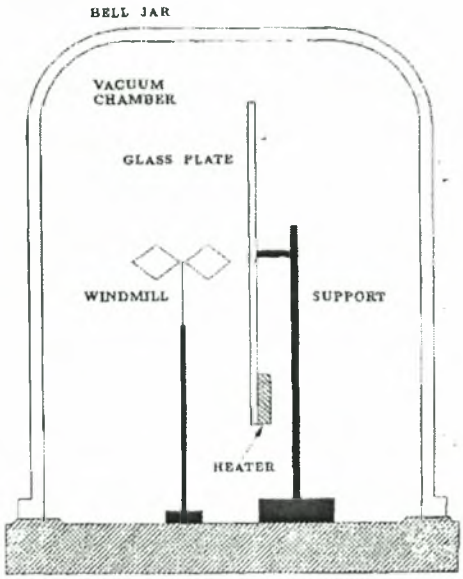

Figure 1.2: Experimental apparatus (Sone, 1991)

With this apparatus, Sone tried to detect a flow induced along the plate by the rotation of the windmill under pressure ranging from atmospheric condition down to about 3 Pa [Sone, 1991].

In recent times, the advent of micro – electro mechanical systems (MEMS) made way for new perspectives on thermal transpiration [Cardenas et al., 2011]. Actually, the interest in the temperature induced flow is growing in connection with micromachine engineering. A pumping system making use of the flow attracts new attention, since such a system has no moving parts and no mixing process. In a rarefied gas in a pipe, whose temperature has a gradient along its axis, a flow is induced in the direction of the gradient, and this flow has a pumping effect [Sone et al., 1996]. The possibility of using the pumping effect of thermal transpiration to create a micro – compressor without moving parts, led to various experimental works by several researchers, in which the attention is mainly focused on the pressure increase due to the application of a temperature gradient along the channel [Cardenas et al., 2011].

1.3 The Knudsen pump

Danish physicist Martin Knudsen introduced a vacuum pump that works for a gas under rarefied conditions or in microscales. This pump is a type of vacuum pump that works by the principle of thermal transpiration, as mentioned above, has no moving parts and offers high reliability [McNamara & Gianchandani, 2003].

A basic configuration of a Knudsen pump consists of two chambers, maintained at different temperatures, connected by a narrow channel that restricts gas flow to the free molecular regime. If the system is sealed, the ratio of equilibrium pressures in the two chambers is nominally given by the ratio of the square root of the respective temperatures, as shown in Eq. (1.9). Knudsen demonstrated a multiple stage thermal transpiration pump, by alternating a series of volumes and tubes [Vargo et al., 1999]. A modern version of this configuration was presented in recent years [Vargo et al., 1999].

The flow of a gas in a grooved channel, due to an imposed temperature gradient in the longitudinal direction, has also been investigated. This flow has common characteristics with the classical Poiseuille flow and is found in thermal creep problems, but the presence of rectangular grooves that are placed periodically in one of the two stationary walls, results in a two dimensional flow pattern [Naris & Valougeorgis, 2006].

The feasibility of making a Knudsen pump by using a two – dimensional channel with a "snaky" shape, has also been investigated. The channel is composed of alternately arranged straight and semicircular segments, with a periodic temperature distribution [Aoki et al., 2007].

1.4 Scope of the present work

In the present work we investigate the basic flow configuration related to a preliminary design of a Knudsen pump. We apply classical kinetic model equations to investigate the rarefied gas flow through a cylindrical tube whose ends are maintained at different temperatures. We consider a monatomic rarefied gas stored in two large reservoirs connected by a cylindrical tube of radius R and length L, as shown in

Figure 1.3. A temperature difference is imposed between the two containers, causing a flow of the gas through the tube. The walls and the gas in the container areas far from the tube are maintained at the same pressure P_0 [Pantazis, 2011]

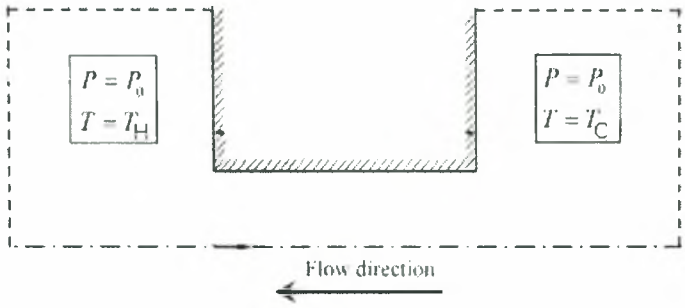

Figure 1.3: Basic flow configuration (Pantazis, 2011)

Our objective is to determine the macroscopic distributions for the whole range of the Knudsen number. This is accomplished by using non-linear kinetic equations. In particular, the flow can be modelled by implementing the nonlinear BGK and Shakhov kinetic equations coupled to Maxwell diffuse boundary conditions [Maxwell, 1879].

The contents of this thesis are as follows: In Chapter 2 a literature review of the kinetic theory and kinetic models developed to approximate the flow is presented. The most important concepts and equations concerning the phenomenon of thermal transpiration are introduced and discussed. Also, available research work solving the specific problem under consideration is discussed. In Chapter 3 we present a description of the problem and the formulation of the corresponding kinetic equations based on the implemented ES model. The simulation of the boundary conditions is also described in this chapter. Finally, the basic macroscopic quantities of interest are presented as well. The numerical scheme is described in Chapter 4. Results regarding the flow are provided in Chapter 5. Also, basic conservation principles and flow properties valid for the whole range of the Knudsen number are derived. Chapter 6 provides an extensive report on several configurations concerning the Knudsen pump. Based on the results that are obtained and presented in Chapter 5, an estimation on a highly reliable Knudsen pump is presented. Finally, in Chapter 7, a brief outline of the

present work, followed by some concluding remarks and the description of future work are presented.

It must be pointed out that the present work is based upon advanced and computationally efficient numerical codes, developed by Dr. S. Pantazis during his Ph. D. studies at the University of Thessaly.

Chapter 2

Literature review

2.1 The phenomenon of thermal transpiration

Investigating the phenomenon of thermal transpiration, or thermal creep, as the basis of a vacuum pump, has a sporadic history since the early 1900s [Vargo et al., 1999]. Thermal transpiration refers to the phenomenon of gas molecules drifting from the cold end to the hot end of a narrow channel subjected to a longitudinal temperature gradient. Reynolds's pioneering investigations of thermal transpiration were closely followed by a rigorous mathematical analysis by Maxwell in 1879. In 1910, Knudsen first proposed the feasibility of a gas pump based on this phenomenon [Gupta & Gianchandani, 2008], and its basic concept is illustrated in Figure 2.1.

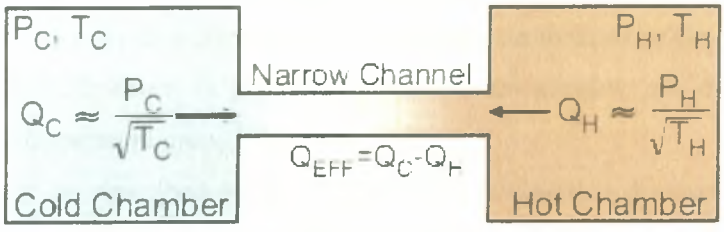

Figure 2.1: Thermal transpiration. If two chambers are connected by a channel that restricts flow to the free - molecular regime, the ratio of pressures at equilibrium is nominally equal to the ratio of the square root of their absolute temperatures (Gupta and Gianchandani, 2008)

Consider two vessels containing a gas at different temperatures T_C, T_H and connected by a capillary. The pressure of both vessels and at all walls remains constant and equal to P_0. To maintain the temperature difference between the vessels, the gas begins to move from the cold vessel to the hot one [Sharipov, 1996]. Our aim is to calculate quantities of practical interest, such as the mass flow rate, in the steady state. Problems of this type have been investigated by various researchers, for several cross – sections and different conditions [Pantazis, 2011].

There are significant applications for such flows and particularly for a flow through cylindrical tubes. In the case of an orifice, i.e. a tube of negligible length, the configuration can be used for comparison with experimental data without the

influence of gas – surface interaction, since the results are practically independent of the wall accommodation properties. Thus, the apparatus can be experimentally realized and used as a test for kinetic models, numerical methods and intermolecular interaction models. Furthermore, orifices and finite length channels are commonly encountered in many practical applications in aerospace engineering, vacuum, microfluidics and other applications, while long channels are also common in vacuum and MEMS networks.

The study of short channels poses large difficulties due to the increased dimensionality of the problem: the distribution function is four- or five – dimensional and the complete flow field, including part of the upstream/downstream containers, must be included in the simulation. In that case the methodology is differentiated [Pantazis, 2011].

The flow through long channels has been considered by many researchers and for various geometries, both numerically and experimentally. The availability of results stems from the simplifications occurring, because of the fully developed flow conditions. Due to this hypothesis, the channel end effects are considered to be negligible. In all these works however, it was assumed that the gradients are so small that the kinetic equation and the boundary conditions can be linearized near the equilibrium state. As a result, a dimensionless flow rate as a function of the Knudsen number is obtained. However, in practice, e.g. in vacuum systems, one deals with large pressure or temperature drops [Sharipov, 1997].

If the system, as described above in Figure 2.1, is closed, a pressure drop is established between the vessels. The pressure drop causes a gas flow which is opposite to the thermal creep so that the whole mass flow through the capillary vanishes in the stationary state. This is the so – called thermomolecular pressure effect.

Pumping energy is supplied by temperature changes alone, as already mentioned. A general feature of such pumps is that the upper pressure limit is reached when the mean free path becomes small relative to the physical dimensions of the pump in the region of the temperature transition. Thus, the upper pressure limits of these pumps have been determined by the microfabrication limits of the day; they have operated at relatively low pressures, with low throughputs, and have not become main line pumps. In recent years, however, Micro-Electronic-Mechanical Systems (MEMS) have introduced a whole new level of miniaturization to devices in general,

including vacuum devices, and hence have raised the upper pressure limits, and thus the throughputs of thermal molecular pumps to atmospheric levels. The general pumping phenomenon has various names: Knudsen compressor; thermal transpiration; thermal creep; thermodynamic, thermomolecular, thermal molecular, and accommodation pumping. Broadly speaking, these pumps divide into two classes: (a) those requiring no specially prepared surfaces, (b) those in which special surfaces are essential. The latter have no low pressure limit [Hobson & Salzman, 2000].

The thermomolecular pressure effect is very important in practice, because in many studies it is necessary to calculate the pressure P_H in a vacuum chamber at a given temperature T_{H1}, from a measured pressure P_C in another chamber at a given temperature T_C. If the chambers are joined by a capillary and the relation of P_H to P_C, T_H, T_C is known, one easily obtains P_H.

The scientific importance of the effect is also significant, because it is sensitive to many properties of the gas such as viscosity, thermal conductivity etc. In that way, it can be used to verify a validity of kinetic models describing both gas – gas and gas – surface interactions. Thermomolecular pressure difference measurements can be used to calculate several thermal properties of polyatomic gases as well. Thus, due to the great practical and scientific importance, the thermal transpiration phenomena continue to attract the attention of theoretical and experimental researchers as well.

As stated before, the relation between P_H, P_C, T_H and T_C in a general form can be written as

$$\frac{P_H}{P_C} = \left(\frac{T_H}{T_C}\right)^{\gamma} \qquad (2.1)$$

where the coefficient γ depends on many factors: the length – to – radius ratio of the capillary, the kind of the gas, and the nature of the gas – surface interaction [Ritos et al., 2011]. But the coefficient γ significantly depends on the Knudsen number defined as $Kn = \lambda/\alpha$, where λ is the mean free path and α is the capillary radius. The mean free path can be related to the pressure and temperature as seen in Section 1.5, of the present thesis.

Thus, for a given gas, the Knudsen number is a function of the pressure and temperature $Kn = Kn(P,T)$ [Sharipov, 1996].

2.2 Thermal creep configurations

2.2.1 Ideal aperture

Figure 2.2 is a simplified drawing of an apparatus of Pyrex glass constructed by Edmonds and Hobson to represent an ideal aperture. Volumes were measured and known. The dashed line represents a sharp transition between T_1 (77.4K at liquid nitrogen or 232K at solid CO_2 mush) and T_2 (room temperature -295K). P_2 is measured by a Bayard – Alpert gage operated at room temperature and at very low electron current. P_1 is not measured directly but deduced by the reduction in P_2 when T_1 is lowered, assuming that the total quantity of gas in the closed system in the gas phase is unchanged. The physical adsorption of helium on Pyrex glass at 77.4K and also of neon is negligible. The inner diameter of the aperture was 20 mm [Hobson & Salzman, 2000].

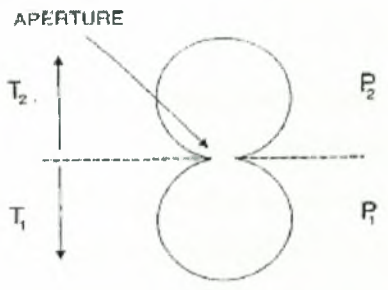

Figure 2.2: Schematic diagram of two volumes at different temperatures joined by an "ideal aperture" (Hobson and Salzman, 1999)

2.2.2 Volumes joined by a tube

A new apparatus was built and is shown schematically in Fig. 2.3, in which the volumes were joined by a long, relative to the radius, Pyrex tube with essentially the same inner diameter as the aperture in Fig. 2.2. It was empirically found that γ varied from Pyrex tube to Pyrex tube. The experimental range was $1.1 < \gamma < 1.3$. Since Pyrex tubes were frequently used for measurements on physical adsorption isotherms in which thermal transpiration corrections were required at low pressures, a material for

the tube was sought with more reproducible characteristics. It was found that Pyrex glass could be leached or roughened [Hobson & Salzman, 2000].

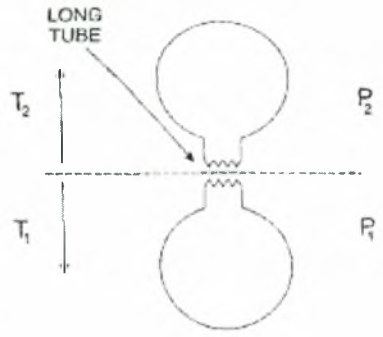

Figure 2.3: Schematic diagram of two volumes at different temperatures joined by a long tube (Hobson and Salzman, 1999)

2.2.3 Accommodation pump

Figure 2.4 shows the first accommodation pump. There are now three volumes: *A* and *B* at room temperature, and *C* at liquid nitrogen temperature. *A* is joined to *C* through a rough tube and *B* is joined to *C* through a smooth tube. It is argued that at equilibrium: $P_A / P_C = (T_2 / T_1)^{1/2}$; $P_B / P_C = (1/\gamma)(T_2 / T_1)^{1/2}$. Hence, $P_A / P_B = \gamma$ is called the compression ratio. The experimental results confirm this prediction [Hobson & Salzman, 2000].

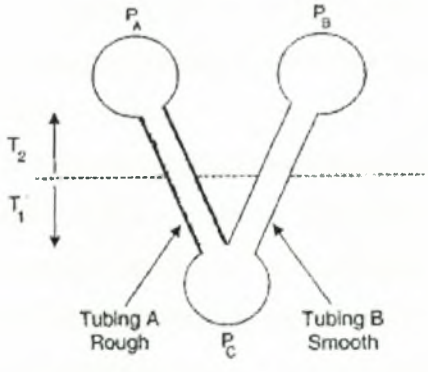

Figure 2.4: Schematic diagram of the first accommodation pump (Hobson and Salzman, 1999)

Baum visualized the thermal transpiration pump operating as a circulation pump in the pressure range of 1 to 10^{-2} Torr with a speed of about 0.1 litre sec^{-1}, or as a forepump for a waterjet pump or a means of extending the range of a vacuum pump. Baum also considered it suitable, with certain modifications, as an isotope separator.

Schumacher et al. considered the device purely as a pump, however, and operated it in the range of 10^{-1} Torr to 10^{-3} Torr and for speeds of about 0.5 to 1.5 litre sec^{-1}.

The theory of thermal transpiration is well known. If two volumes are connected by a tube with dimensions less that the mean free path of the gas molecules, and the ends of the connecting tubes are kept at different temperatures, then a pressure differential is set up between the ends of the tube, such that the pressure ratio equals the square root of the temperature ratio. This relationship represents the equilibrium condition, under which there is no net gas flow along the tube.

In order that the throughput of the pump is not too small, the connecting tubes should be as large in cross – sectional area as possible, and this clashes with the requirement that molecular flow be established in them. Baum overcame this by making the tube annular in cross section; thus, its area was large while its width was small [Turner, 1966].

Pham – Van – Diep et al. first outlined a microelectromechanical systems (MEMS) based thermal transpiration Knudsen compressor. Later on, Vargo et al. presented a device that is a modern version of Knudsen's thermal transpiration compressor. A Knudsen compressor generates large changes in pressure by utilizing a cascade of multiple stages. Each stage is composed of a capillary and connector section. A temperature increase across the capillaries results in a thermal transpiration driven, pressure increase. The capillary section is followed by a connector section where the pressure is approximately constant, while the temperature drops to its original value entering the stage.

The original analysis of a Knudsen compressor's performance was based on the assumption of an ideal situation of free – molecule flow in the capillary section and continuum flow in the connector section of a compressor stage. While these conditions can be closely matched in laboratory compressors, it is expected in practice that both the capillary and the connector sections of the compressor frequently will operate in the transitional flow regime [Vargo et al., 1999].

Naris and Valougeorgis also investigated the flow of a gas in a grooved channel, due to imposed temperature and pressure gradients in the longitudinal direction. The flow has common characteristics with the classical Poiseuille flow and thermal creep problems, but the presence of the rectangular grooves that are placed periodically in one of the two walls, results in a two – dimensional flow pattern. The objective was to solve both the pressure and the temperature driven problems in the whole range of the Knudsen number, and a kinetic approach based on the Shakhov model was followed. They also studied pressure and temperature driven flows through triangular and trapezoidal microchannels, giving special attention to the computation of the coefficient of the thermomolecular pressure difference [Naris & Valougeorgis, 2006].

Aoki et al. investigated the feasibility of constructing a Knudsen pump by changing the curvature of the channel instead of changing its cross – sectional area. They showed that a two – dimensional channel with a "snaky" shape, as shown in Figure 2.5, composed of alternately arranged straight semicircular segments, with a periodic temperature distribution, has a pumping effect [Aoki et al., 2007].

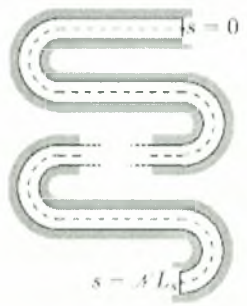

Figure 2.5: Snaky cascade system (Aoki et al., 2007)

A major challenge in the design of thermal transpiration based pumps is to ensure good thermal isolation between the hot and cold ends of the pump in order to maximize the thermal difference.

The primary parameters affecting the thermal isolation are the thermal conductivity of the pump channel material, and the length of the channel separating the hot and the cold sides. Although a longer channel will improve the thermal isolation, a longer channel also increases the gas flow impedance, requiring the making of a tradeoff. Typically, a Knudsen pump uses a resistive heater to actively heat the hot side and the cold side is passively cooled by means of a heat sink.

A novel technique to create a vacuum pump on an integrated circuit chip was presented by R. M. Young. This pump consists of small tubes operating in the free molecular regime, connected to larger, although still miniature, viscous flow chambers. The gas is alternately heated and cooled as it traverses these tubes and chambers, with the thermal transpiration effect creating a mass flow and compression in each stage [Young, 1999].

A novel solution to attaining a large thermal difference was presented by Pharas and McNamara. They first used a thermoelectric material in the bidirectional operation of a gas pump using thermal transpiration. The thermoelectric material maintains a higher temperature difference which favours thermal transpiration and thus increases the efficiency of gas pumping [Pharas & McNamara, 2010].

Although the phenomenon of thermal transpiration has been known for more than a century, very few efforts have focused on the atmospheric pressure operation of a Knudsen pump, because this requires channels with hydraulic diameter smaller than approximately 100 nm. Vargo and Muntz first reported a mesoscale device for operation near atmospheric pressure using nanoporous aerogel, providing a best case pressure drop of 11.5 Torr (≈1.5 kPa) using helium [Vargo et al., 1999, Hobson & Salzman, 2000].

McNamara and Gianchandani reported the feasibility of using lithographically patterned nanochannels in a chipscale, fully micromachined, Knudsen pump that achieved a pressure drop of about 54.7 kPa with 80 mW of input power. However, the limitation on the density of lithographically patterned narrow channels in a micromachined Knudsen pump constrains the flow rate to the order of 10^{-6} cc/min. Also, in their 2008 work, Gupta and Gianchandani explored the use of a naturally occurring zeolite, clinoptilolite, for a chip-scale, thermal transpiration-based gas pump [Gupta & Gianchandani, 2008].

Chapter 3

Problem description and formulation

3.1 Introduction

Studies have shown that an unconventional solid state device, the Knudsen compressor, can be operated as a micro-scale pump or compressor over a pressure range from several atmospheres down to about 10 mTorr. The critical components of Knudsen compressors are gas transport membranes, which can be formed from materials with randomized (porous) flow channels to densely packed parallel arrays of multiple individual flow channels. In the computational studies several approaches have been employed: the direct simulation Monte Carlo (DSMC) method, and discrete ordinate solutions of the ellipsoidal statistical (ES) and Bhatnagar – Gross - Krook (BGK) kinetic models. The ES kinetic model permits accurate descriptions of temperature gradient driven flows, easily resolving flow velocities of well under a few meters per second for reasonable computational costs [Pantazis, 2011].

It must be noted that there are some basic requirements, for the construction of a kinetic model, and these are the following:

- The laws of conservation must be satisfied
- The distribution function should approach the Maxwellian distribution in equilibrium
- Results near the hydrodynamic regime should agree with exact results known for that case
- The H-Theorem must be satisfied

The BGK model was the first model to appear and has been widely applied, mostly due to its simplicity:

$$Q(f, f^M) = \nu(f^M - f) \quad (3.1)$$

with ν being the collision frequency, assumed to be independent of the molecular velocity, and f^M is the local Maxwellian, calculated with the local number density,

temperature and velocity according to Equation (3.1). The Maxwellian and local distribution parts represent the gain and loss terms of the Boltzmann collision operator, respectively. This model is closely related to the Maxwell diffuse type of reflection for interaction with walls, since molecules relax to the local Maxwellian distribution with a uniform angular distribution around the point of collision after a single collision.

The BGK model has provided satisfying results in the whole range of the Knudsen number. In fact, it has been seen in many works that the results provided by this model are reasonably close to the ones provided by the Boltzmann equation (e.g. within 1-2%). However, there are some well known limitations of the model. In particular, the collision frequency must be adjusted according to the flow needs. For an isothermal flow, a Chapman-Enskog expansion method is used to obtain the correct value of viscosity, while for non-isothermal transport phenomena the heat conductivity is matched to the value provided by the full collision integral by the same method. It is impossible to have simultaneously both transport coefficients correctly determined by this model and therefore it yields a Prandtl number equal to unity for monatomic gases (the correct value is 2/3). In the BGK model, the collision frequency must be multiplied by 3/2 for the solution of heat transfer problems and therefore it is not appropriate for the simulation of coupled flow and heat transfer phenomena.

Two more models were produced in the same manner but also keeping higher moments of the collision term, namely the Shakhov model

$$Q(f,f_S)=\frac{P}{\mu}\left\{f^M\left[1+\frac{2}{15}\frac{m}{n(k_BT)^2}\boldsymbol{q}\cdot(\boldsymbol{\xi}-\boldsymbol{u})\left(\frac{m(\boldsymbol{\xi}-\boldsymbol{u})^2}{2k_BT}-\frac{5}{2}\right)\right]-f(t,\boldsymbol{r},\boldsymbol{\xi})\right\} \quad (3.2)$$

and the ellipsoidal model

$$Q(f,f_{ES})=\frac{P}{\mu}\Pr\left\{\frac{n}{\pi^{3/2}}\sqrt{|A|}\exp\left[-\sum_{i,j=1}^{3}(\xi_i-\bar{u}_i)A_{ij}(\xi_j-\bar{u}_j)\right]-f\right\} \quad (3.3)$$

where $$A_{ij} = \left[\frac{2k_B T}{m \Pr} \delta_{ij} - \frac{2(1-\Pr)\bar{P}_{ij}}{nm \Pr} \right]^{-1} \qquad (3.4)$$

In the above expressions, Pr is the Prandtl number, k_B is the Boltzmann constant, m is the molar mass and δ_{ij} the Kronecker delta. The ellipsoidal model is derived to further satisfy the expression

$$\int (\xi_i - \hat{u}_i)(\xi_j - \hat{u}_j) f_{ES} d\xi = \frac{nk_B T}{\Pr} \delta_{ij} - \frac{(1-\Pr)\bar{P}_{ij}}{\Pr} \qquad (3.5)$$

It can be seen that by substituting Pr = 1 in (3.2) and (3.3) the BGK expression is retrieved. In the simulations the characteristic value for monatomic gases, Pr = 2/3, has been used to obtain the correct values for all physical quantities.

A shortcoming of the Shakhov model is that the H-theorem has not been proven in its nonlinear form. However, since it was shown that the H-theorem holds for the ES model, it is believed that it also holds for the S model since they have been produced in the same manner.

It is also important to note that it is sometimes possible to linearize the distribution function in terms of a small quantity depending on the problem at hand (e.g. a small pressure gradient in a pressure driven flow). In this case, the resulting equations are easier to handle and possess favourable mathematical properties. Furthermore, similar equations have been widely used in the past in neutron transport problems and this leads to an exchange of concepts and methods [Pantazis, 2011].

3.2 Geometry of the problem under consideration and governing equations

Consider two large reservoirs connected by a cylindrical tube of radius R and length L, as shown in Figure 3.1. The two reservoirs containing a rarefied gas at temperatures T_C and T_H and maintained at pressure P_0 are connected via a channel through which the gas flows. The reservoirs are infinitely large and only a fraction of

their real size is shown here. The position vector $x = (x_1, x_2, x_3)$ refers to (x, y, θ) with a characteristic length $L_0 = R$, where R is the tube radius. The flow is oriented towards the positive direction of the x coordinate. Due to the geometrical properties of the flow, the dependence on the component x_3 is also omitted. Finally, the velocity vector is denoted by $c = (c_1, c_2, c_3)$ and the component orientations are identical to the ones of the corresponding coordinates in the physical space.

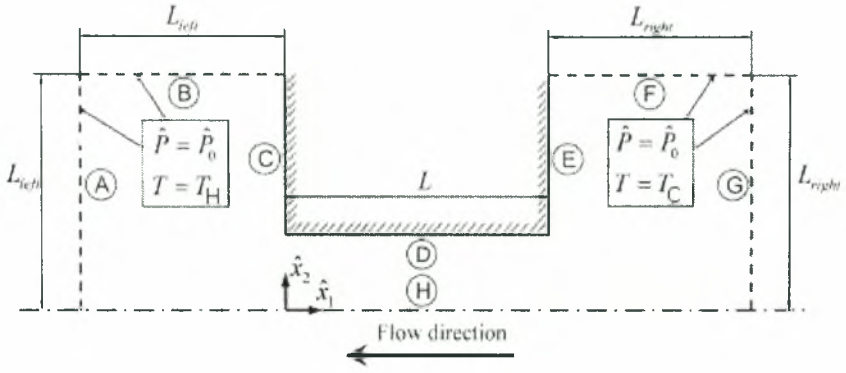

Figure 3.1: Flow configuration and coordinate system

It must be noted that the complete geometry is simulated, including the part of the containers before and after the channels. This type of investigation is possible for short to moderately long channels, and has been realized here for a cylindrical tube. Two cases are investigated with the channel length being 10 and 50 times the tube radius respectively.

The molecular velocity coordinate system is shown in Figure 3.2, below.

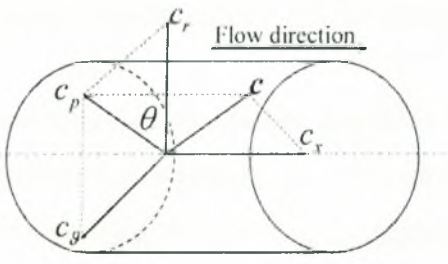

Figure 3.2: Velocity coordinate system for the tube problem

The symbol ϑ denotes the direction perpendicular to the $\bar{r}$ - $\bar{x}$ plane, while θ is the molecular velocity angle in the $\bar{r}$ - ϑ plane. The computational domain includes a

part of the containers upstream and downstream of the tube, since the channel is relatively short and the effects of flow entrance and exit need to be taken into account.

The starting point is the ES kinetic model equation, which has been found to exhibit significant advantages in comparison to its predecessor, the BGK model, such as the adjustment of the Prandtl number. In cylindrical coordinates it is expressed by

$$\xi_r \frac{\partial f}{\partial \bar{r}} - \frac{\xi_\theta}{\bar{r}} \frac{\partial f}{\partial \theta} + \xi_x \frac{\partial f}{\partial \bar{x}} = \nu\left(f^{ES} - f\right) \quad (3.6)$$

with $f = f\left(\bar{r}, \bar{x}, \xi_r, \xi_\vartheta, \xi_x\right)$ being the distribution function and ν is the collision frequency. The collision term is retained in its non – linear form with

$$f^{ES} = \frac{n}{\pi^{3/2}} \sqrt{|A|} \exp\left[- \sum_{i,j=1}^{3} \left(\xi_i - \bar{u}_i\right) A_{ij} \left(\xi_j - \bar{u}_j\right) \right] \quad (3.7)$$

where

$$A_{ij} = \left[\left(2 k_B T \delta_{ij} / m \Pr\right) - 2\left(1 - \Pr\right) \bar{P}_{ij} / nm \Pr \right]^{-1}$$

as stated above in the Equation (3.4). Pr is the Prandtl number, k_B is the Boltzmann constant, m is the molar mass and δ_{ij} the Kronecker delta. Also, n, T, $\bar{u}$, $\bar{P}_{ij}$ are the number density, temperature, gas bulk velocity and stress tensor components, respectively. By substituting Pr = 1, the BGK expression is obtained. The characteristic value for monatomic gases, i.e. Pr = 2/3, has been used in the following calculations.

The left reservoir conditions, i.e. the number density n and pressure P, are chosen as reference quantities and are denoted by n_0, P_0, with $P_0 = n_0 k_B T_0$ from the ideal gas law. All quantities of practical interest are non – dimensionalized as follows:

$$r = \frac{\bar{r}}{R}, \; x = \frac{\bar{x}}{R}, \; \mathbf{c} = \frac{\xi}{\upsilon_0}, \; g = \frac{f \upsilon_0^3}{n_0}, \; \rho = \frac{n}{n_0}, \; \boldsymbol{u} = \frac{\bar{\boldsymbol{u}}}{R}$$

$$\tau = \frac{T}{T_0},\ q = \frac{\tilde{q}}{P_0 \upsilon_0},\ P = \frac{\hat{P}}{P_0},\ P_{ij} = \frac{\hat{P}_{ij}}{P_0},\ i,j = r,\vartheta,x \quad (3.8)$$

with $\upsilon_0 = \sqrt{2k_B T_0 / m}$ being the most probable molecular velocity and $\tilde{q}$ being the heat flux vector.

The collision frequency is given by the expression

$$\nu = \frac{P}{\mu}\Pr \quad (3.9)$$

where μ is the dynamic viscosity. The reference rarefaction parameter δ_0 is defined as

$$\delta_0 = \frac{P_0 R}{\mu_0 \upsilon_o} = \frac{\sqrt{\pi}}{2}\frac{1}{Kn_0} \quad (3.10)$$

It is inversely proportional to the Knudsen number and therefore as δ_0 increases the atmosphere becomes more dense (or less rarefied). The cases of δ_0 = 0 and $\delta_0 \to \infty$ correspond to the free molecular and the hydrodynamic limits respectively.

It is seen that the distribution function $g = g(x,r,c_r,c_\vartheta,c_x)$ cannot be projected in the velocity space, because all molecular velocity components are required. As a result, g depends on a total of five dimensions. The velocity vector is transformed into cylindrical coordinates $c = (c_p,\theta,c_x)$ and the final form of the governing equation is

$$c_p \cos\theta \frac{\partial g}{\partial r} - \frac{c_p \sin\theta}{r}\frac{\partial g}{\partial \theta} + c_x \frac{\partial g}{\partial x} = \delta_0 \rho \sqrt{\tau}\,\Pr\left(g^{ES} - g\right) \quad (3.11)$$

where the dimensionless ES model term becomes

$$g^{ES} = \frac{\rho}{\pi^{3/2}}\Pr^{3/2}\sqrt{|K|}\exp\left[-\Pr\sum_{i,j=1}^{3}(c_i - u_i)K_{ij}(c_j - u_j)\right] \quad (3.12)$$

with

$$K = \left[\tau\delta_{ij} - (1-\mathrm{Pr})P_{ij}/\rho\right]^{-1} \quad (3.13)$$

We only examine velocity angles in $\theta \in [0,\pi]$ since the distribution function is axisymmetric [Pantazis, 2011].

3.3 Macroscopic quantities

The macroscopic quantities are also non – dimensionalized, leading to the following expressions:

$$\rho = 2\int_0^\infty\int_0^\pi\int_{-\infty}^{\infty} c_p g dc_x d\theta dc_p \quad (3.14)$$

$$\tau = \frac{4}{3\rho}\int_0^\infty\int_0^\pi\int_{-\infty}^{\infty} c_p\left[(c_p\cos\theta - u_r)^2 + (c_p\sin\theta)^2 + (c_x - u_x)^2\right] g dc_x d\theta dc_p \quad (3.15)$$

$$u_x = \frac{2}{\rho r}\int_0^\infty\int_0^\pi\int_{-\infty}^{\infty} c_p c_x g dc_x d\theta dc_p \quad (3.16)$$

$$u_r = \frac{2}{\rho r}\int_0^\infty\int_0^\pi\int_{-\infty}^{\infty} c_p^2\cos\theta g dc_x d\theta dc_p \quad (3.17)$$

$$P_{ij} = 2\int_0^\infty\int_0^\pi\int_{-\infty}^{\infty} c_p(c_i - u_i)(c_j - u_j) g dc_x d\theta dc_p \quad (3.18)$$

$$q_x = 2\int_0^\infty\int_0^\pi\int_{-\infty}^{\infty} c_p\left[(c_p\cos\theta - u_r)^2 + (c_p\sin\theta)^2 + (c_x - u_x)^2\right](c_x - u_x) g dc_x d\theta dc_p \quad (3.19)$$

$$q_r = 2\int_0^\infty\int_0^\pi\int_{-\infty}^{\infty} c_p\left[(c_p\cos\theta - u_r)^2 + (c_p\sin\theta)^2 + (c_x - u_x)^2\right](c_p\cos\theta - u_r) g dc_x d\theta dc_p \quad (3.20)$$

Vector/tensor components containing the ϑ -direction once, i.e. $u_\vartheta, p_{r\vartheta}, p_{z\vartheta}, q_\vartheta$, are equal to zero, while $p_{\vartheta\vartheta}$ is not. Pressure can be obtained by $P = \rho\tau$.

The main quantity of interest is the mass flow rate through the tube $\dot{M}$ and our aim is to calculate it for a wide range of the parameters characterizing the flow: the reference rarefaction parameter δ_0, the channel aspect ratio L/R and the temperature ratio T_C/T_H. For the current problem, the mass flow rate is calculated by

$$\dot{M} = 2\pi \int_0^R [mn(\bar{x},\bar{r})]\bar{u}_x(\bar{x},\bar{r})\bar{r}d\bar{r} \quad (3.21)$$

The flow rate given by Equation (3.21) is non - dimensionalized according to (3.8)

$$\dot{M} = 2\pi(mn_0)(\upsilon_0)(R^2)\int_0^1 \rho(x,r)u_x(x,r)rdr \quad (3.22)$$

Then we multiply and divide with $\upsilon_0 = \sqrt{2(k_B/m)T_0}$ and use the ideal gas law $P_0 = n_0 k_B T_0$ to get

$$\upsilon_0 = 2\pi R^2 \frac{2P_0}{\upsilon_0}\int_0^1 \rho(x,r)u_x(x,r)rdr \quad (3.23)$$

Finally, dividing by the pressure driven, free molecular solution $\dot{M}_{FM} = R^2\sqrt{\pi}\,\bar{P}_{in}/\upsilon_0$ we get the dimensionless flow rate

$$W = \frac{\dot{M}}{\dot{M}_{FM}} = 4\sqrt{\pi}G \quad (3.24)$$

where the reduced flow rate is defined as the integral

$$G_x = \int_0^1 \rho(x,r)u_x(x,r)rdr \quad (3.25)$$

Chapter 4

Numerical scheme

4.1 Introduction

In this chapter, we describe the typical numerical algorithm used to obtain our results. The main characteristic of the numerical scheme are similar to the ones found in previously formulated discrete velocity schemes. The continuum spectrum of the molecular velocity magnitudes c_z and c_r is discretized to M values, their values being chosen according to the roots of the M^{th} order Legendre polynomial mapped in [0, $c_{z,max}$] and [0, $c_{r,max}$] respectively, while the molecular velocity angles N_θ are uniformly distributed in [0,2π], [0, π] for the tube, due to the axisymmetric properties of the flow. The distribution functions, bulk quantity fields and governing equations are further discretized by a finite volume scheme in the physical space for $N_x \times N_r$ points.

The discrete velocity method algorithm is then applied, consisting of the following steps:

i. Bulk quantity perturbations ρ, u and τ are initially assumed
ii. The discretized equations are solved using a marching scheme
iii. New estimations for the bulk quantities are calculated
iv. Steps (ii) and (iii) are repeated until convergence is reached for the macroscopic quantities

The kinetic equation is discretized according to the second order finite volume scheme. At each interval Δr_i, $\Delta\theta_j$, Δx_k around r_i, θ_j, x_k, we act upon the governing equation with

$$A = \int_{x_k-\frac{\Delta x_k}{2}}^{x_k+\frac{\Delta x_k}{2}} \int_{\theta_j-\frac{\Delta\theta_j}{2}}^{\theta_j+\frac{\Delta\theta_j}{2}} \int_{r_i-\frac{\Delta r_i}{2}}^{r_i+\frac{\Delta r_i}{2}} (\cdot)\, dr\, d\theta\, dx \qquad (4.1)$$

to eliminate all derivatives. Then, all integrations can either be carried out analytically or substituted by the trapezoidal rule.

The kinetic equations are solved independently for each velocity component if the macroscopic quantities are known. A marching scheme is applied to solve these equations to avoid solving a system, maximizing efficiency and reducing memory consumption. This is highly desirable, since the tube problem is five – dimensional and therefore subject to significant computational limitations.

The description for the cylindrical geometry marching scheme is briefly described here (Figure 4.1, below).

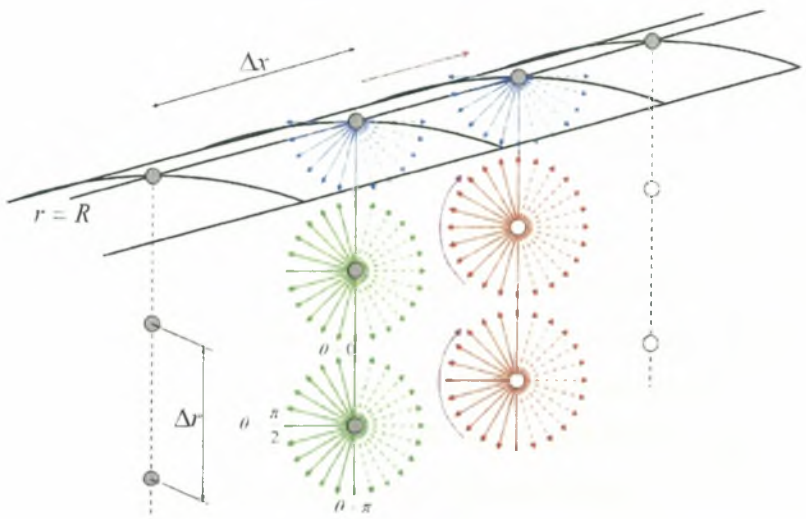

Figure 4.1: Schematic representation of the tube marching scheme

The discretized equation is solved for the unknown values (white nodes) using the known quantities (dark nodes) from the previous column (green arrows) or the boundary conditions (blue arrows). However, we must also take into account the additional complexity of the angular velocity component. The angles are calculated starting from $\theta = \pi$, where a simplified version of the discretized equation can be applied, solving all the way through until the lower boundary. Then, angles starting from $\theta = \pi - \Delta\theta$ down to $\theta = \pi/2$ are calculated in this sequence (as the purple arrow indicates) while moving downwards. The symmetry condition is applied at the center and thus the boundary values for $\theta = \pi/2$ down to $\theta = 0$. Finally, we solve for these distributions until we reach the upper surface. Angles in $(\pi, 2\pi)$ are symmetric and do not need to be calculated again. By taking the discretized version of

the moments of the macroscopic perturbations, employing Gauss – Legendre quadrature for the velocity magnitudes and the trapezoidal rule for the angles, macroscopic quantities are calculated and this procedure is repeated for all columns and each combination of c_z, c_r until the complete macroscopic field has been found.

The application of this algorithm has two important consequences: First, memory requirements are dramatically reduced, since two temporary arrays of dimensions (N_r, N_θ) can be used for the distribution function in the current and the previous column instead of one large with dimensions (N_x, N_r, M, N_θ, M) (which would also be more costly to access in memory due to the multiple dimensions). Storing the distribution only in parts of the domain needed by the marching scheme allows the simulation of much larger and denser grids. Second, the velocity magnitude independency leads to a straightforward parallelization of the code. Each processor solves the kinetic equation for a group of velocities and information on macroscopic quantities and impermeability constants is exchanged between the processors at the end of each iteration. In this manner, the transmission of the distribution function is circumvented, greatly reducing the cost of parallel communication. A large number of processors, namely $M \times N_\theta/2$ and M^2, can be used for the tube problem respectively.

It has also been seen that the convergence rate benefits significantly by adjusting the initial assumption for the macroscopic variables to reasonable values. For example, in the problems of linearized flow through a channel or tube, the density perturbation is chosen equal to unity in the left vessel, zero in the right and varies linearly inside the channel. In the same context, velocities are set to zero everywhere in the field. This selection is quite close to the final expected distribution of macroscopic variables and significantly reduces the number of iterations.

Chapter 5

Results and discussion

5.1 Numerical parameters

The geometric parameters used for the tube geometry are presented in the following table:

Table 1: Geometric parameters

δ	0	0.1	1	5
T_C/T_H	0.1		0.5	
L/R	1		5	

The numerical parameters used in the simulations can be seen in Table 2.

Table 2: Numerical parameters

Numerical Parameters	
Number of discrete angles N_θ	80
Number of grid changing steps	5
Discrete magnitudes of radial velocity	16
Discrete magnitudes of axial velocity	16
Convergence criterion	10^{-6}
Size of the reservoirs connected to the tube	8×8

In Table 3, the required CPU time in minutes is presented, as well as the number of iterations necessary to complete each case, for 16 different runs. It is observed that, in each case of L/R, CPU time and the number of iterations are drastically reduced as the temperature ratio increases and as the value of δ decreases.

Table 3: Total CPU time in hours and number of iterations for each case

	$T_C/T_H = 0.1$				$T_C/T_H = 0.5$			
	L/R=1		L/R=5		L/R=1		L/R=5	
δ	CPU time (hr)	Iterations	CPU time (hr)	Iterations	CPU time (hr)	Iterations	CPU time (hr)	Iterations
0.0	16.7	4	25.9	6	8.9	2	14.4	3
0.1	> 99	22	> 99	21	18.3	4	19.05	4
1.0	> 379	82	> 417	88	> 58	13	> 37	7
5.0	> 1405	183	> 1330	98	> 152	28	> 79	11

5.2 Flow rates

The dimensionless flow rates, obtained for each case can be seen in the following table (Table 4). The "minus" sign is related to the coordinated system for the tube problem, and indicates that the direction of the flow is from the right (cold side) reservoir to the left reservoir (hot side).

Table 4: Dimensionless flow rates (80 discrete angles were used in the simulation)

	$T_C/T_H = 0.1$		$T_C/T_H = 0.5$	
δ	L/R=1	L/R=5	L/R=1	L/R=5
0.0	-1.454	-0.670	-0.278	-0.128
0.1	-1.211	-0.487	-0.265	-0.117
1.0	-0.545	-0.188	-0.190	-0.072
5.0	-0.188	-0.061	-0.088	-0.029

For benchmarking purposes, the problem was further investigated by using 120 and 160 discrete angles respectively, instead of 80, for smaller values of the rarefaction parameter. As we can see in Tables 5 and 6, excellent agreement is demonstrated in all cases.

Table 5: Dimensionless flow rates (120 discrete angles were used in the simulation)

	$T_C/T_H = 0.1$	$T_C/T_H = 0.5$
δ	L/R=1	L/R=1
0.0	-1,45463570	-0,27854670
0.1	-1,21114860	0,26546480

Table 6: Dimensionless flow rates (160 discrete angles were used in the simulation)

	$T_C/T_H = 0.1$	$T_C/T_H = 0.5$
δ	L/R=1	L/R=1
0.0	-1,45463710	-0,27854690
0.1	-1,21113720	-0,26546410

5.3 Macroscopic distributions

Results for the bulk quantities of axial and radial velocity, axial and radial heat flux, temperature and density are presented in this section (Figures 5.1 – 5.16), in terms of the three dimensionless parameters describing the flow, namely the rarefaction parameter δ, the temperature ratio T_C/T_H and the channel aspect ratio L/R.

Observing Figures 5.1 to 5.16 we see that, in all cases, the axial velocity decreases as the length of the tube increases, which shows that the phenomenon is occurring at a slower pace in the case of channel aspect ratio $L/R = 5$ than in the case of $L/R = 1$. As the temperature ratio increases from $T_C/T_H = 0.1$ to $T_C/T_H = 0.5$ we can see that the temperature inside the tube increases as well, showing that the phenomenon becomes more intense in the latter case. Also, the axial heat flux is always positive, denoting, as expected, that heat is moving from the cold side to the hot side of the tube.

We can also observe that, in all cases, the density decreases as the rarefaction parameter increases, while the temperature increases. As the length of the tube increases, density increases as well, while as the temperature ratio is increased, density decreases significantly and temperature increases.

No significant changes are observed in the radial velocities or the radial heat fluxes, indicating that the flow is mainly in the axial direction. However, it can be seen that the velocity component in the radial direction is non – zero, as well as the radial heat flux, something that shows that the flow is not fully developed.

We present the complete set of results related to the distributions so that it may be conveniently useful for reference or future work. However, a comparison between all these results can be performed more easily if we observe Figure 5.17.

In Figures 5.18 – 5.19 we can see the density and temperature distributions for the tube geometry with $\delta = 0.1$ at (a) $L/R = 1$, $T_C/T_H = 0.1$, (b) $L/R = 1$, $T_C/T_H = 0.5$, (c) $L/R = 5$, $T_C/T_H = 0.1$ and (d) $L/R = 5$, $T_C/T_H = 0.5$, respectively. In Figure 5.20 we can see the streamlines, for each case. It is clearly seen that, in all cases, the gas is moving from the cold side (i.e. the right reservoir) to the hot side (i.e. the left reservoir), indicating the presence of thermal transpiration.

5.4 Dimensional flow rates

In this section, some indicative dimensional results are provided. Assuming we have a tube radius equal to 1 μm, we use Equation (1.8) to calculate the pressure for various values of the rarefaction parameter δ. We then calculate the free – molecular solution by using the, already mentioned in section 3.3, relationship

$$\dot{M}_{FM} = R^2 \sqrt{\pi}\, \hat{P}_{in} / \upsilon_0$$

Finally, by using Equation (3.24) we get the dimensional flow rate.

In Table 7, we can the dimensional flow rates obtained for three different values of the rarefaction parameter δ.

Table 7: Dimensional flow rates

	$T_C/T_H = 0.1$		$T_C/T_H = 0.5$	
δ	L/R=1	L/R=5	L/R=1	L/R=5
0.1	4.89E-12	1.97E-12	1.07E-12	4.73E-13
1.0	2.20E-11	7.60E-12	7.68E-12	2.91E-12
5.0	3.80E-11	1.23E-11	1.78E-11	5.86E-12

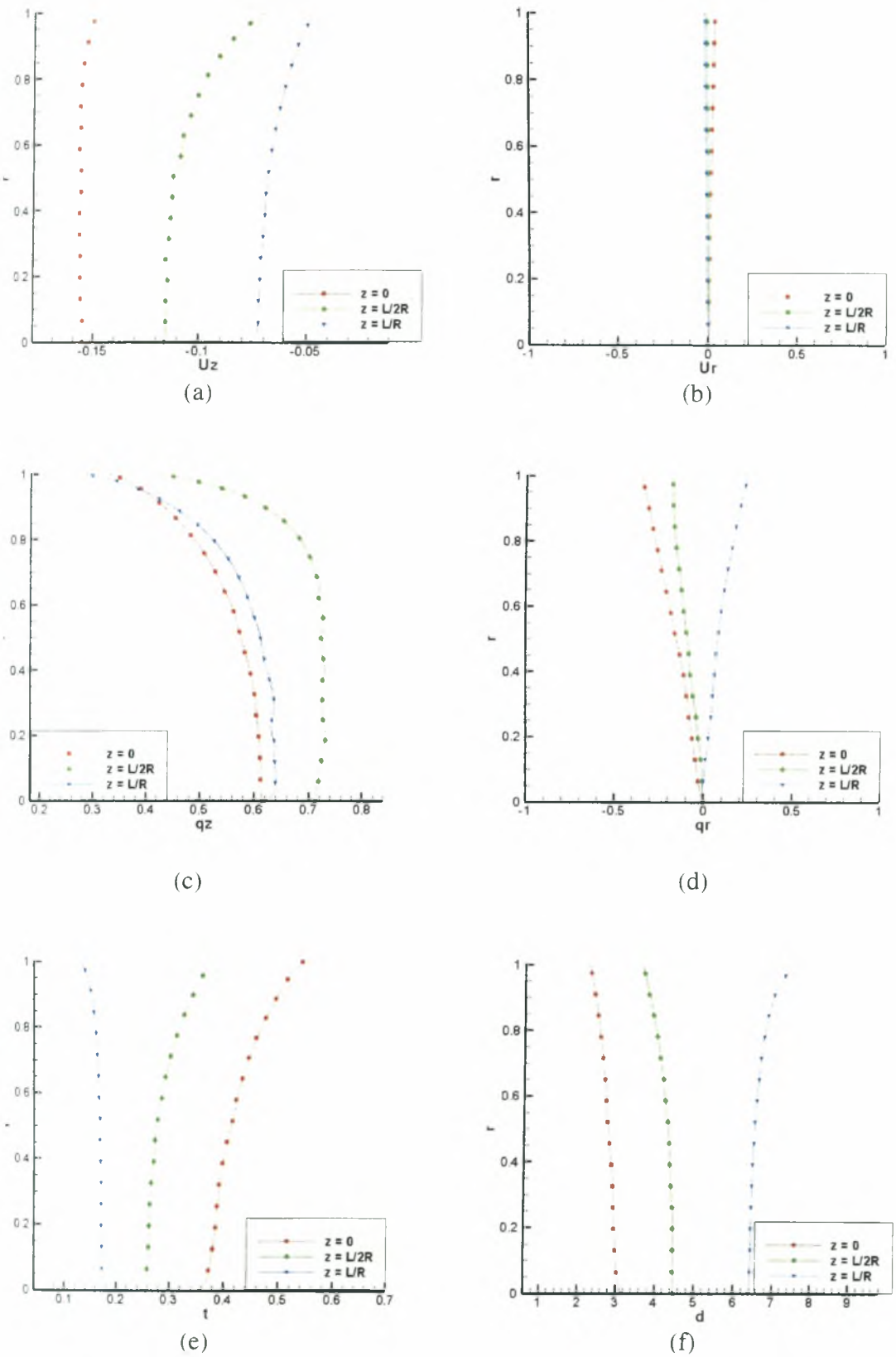

Figure 5.1: Macroscopic distributions along the tube with $L/R = 1$, $T_C/T_H = 0.1$ and δ=0.
(a) Axial velocity, (b) radial velocity, (c) axial heat flux, (d) radial heat flux, (e) temperature and (f) density

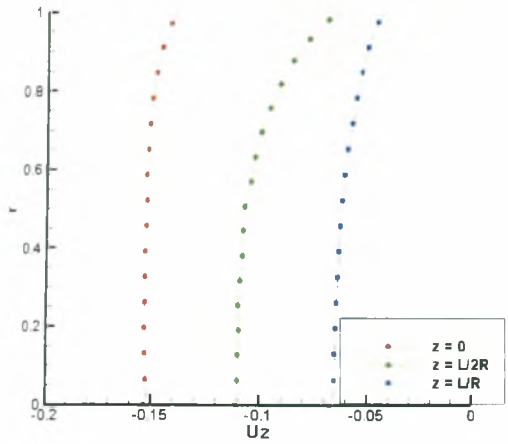

(a)

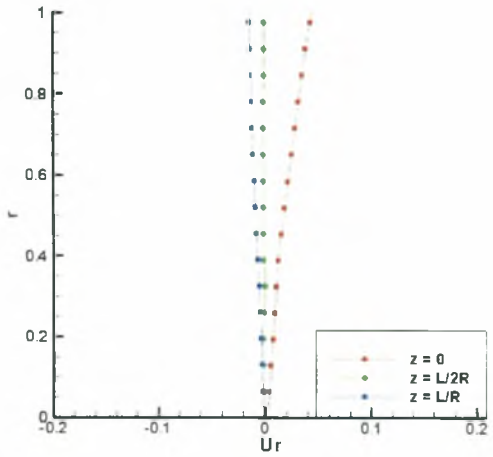

(b)

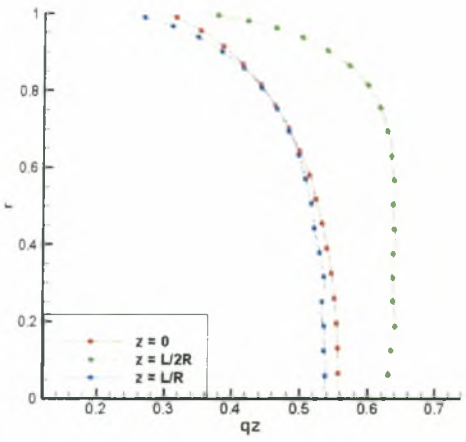

(c)

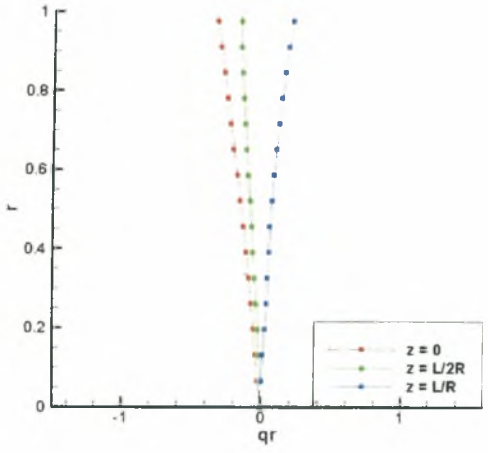

(d)

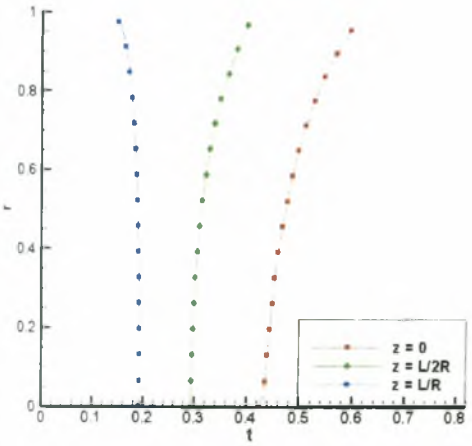

(e)

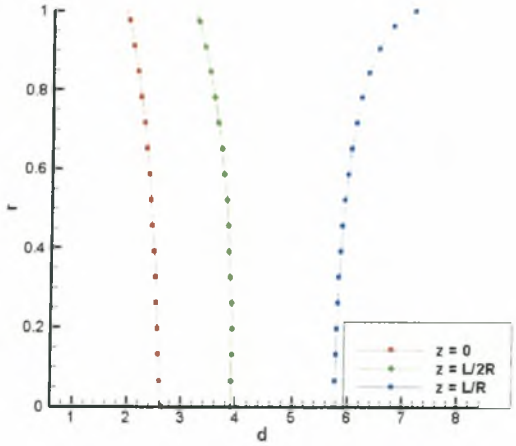

(f)

Figure 5.2: Macroscopic distributions along the tube with $L/R = 1$, $T_C/T_H = 0.1$ and δ=0.1.
(a) Axial velocity, (b) radial velocity, (c) axial heat flux, (d) radial heat flux, (e) temperature and (f) density

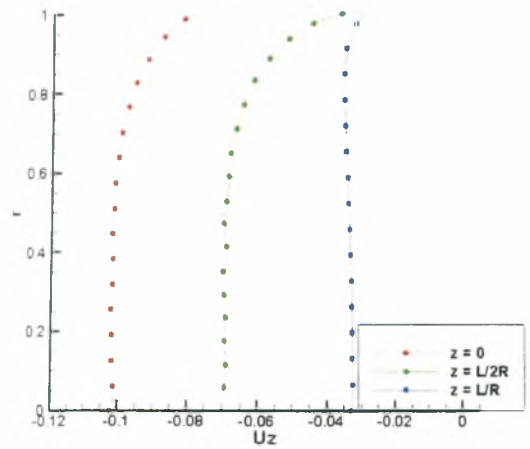

(a)

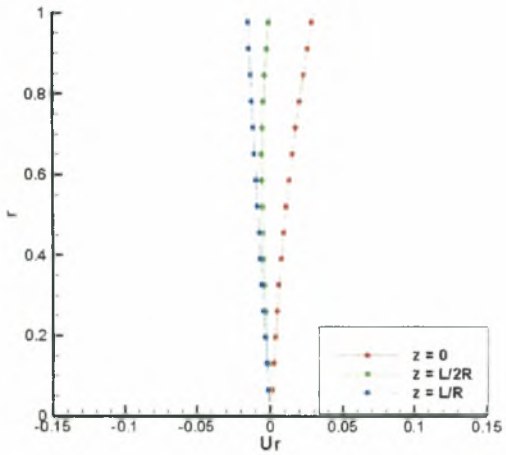

(b)

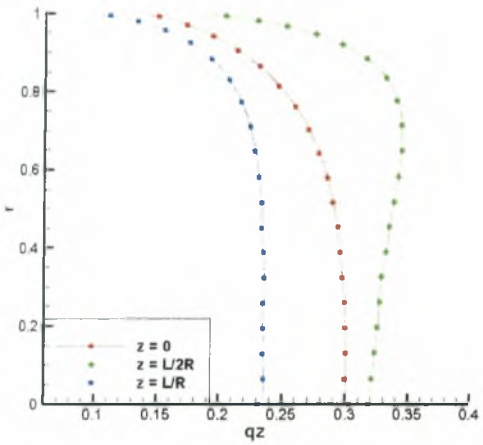

(c)

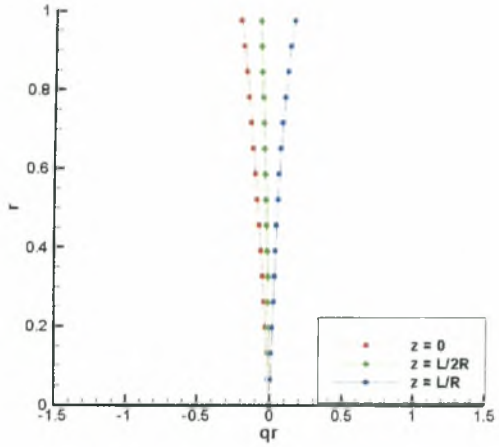

(d)

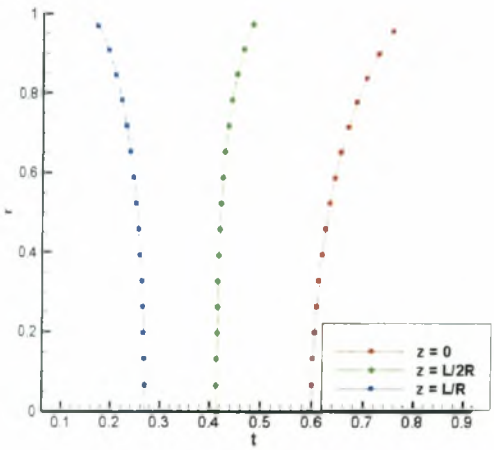

(e)

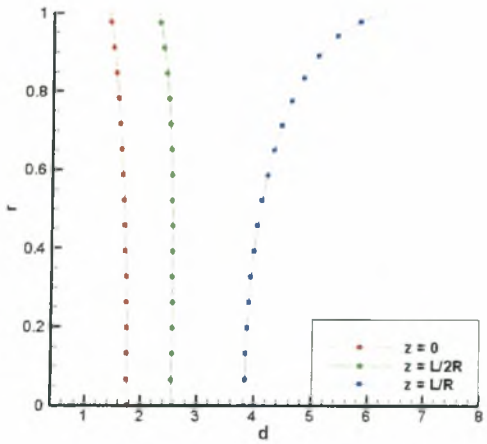

(f)

Figure 5.3: Macroscopic distributions along the tube with L/R = 1, T_C/T_H = 0.1 and δ=1.
(a) Axial velocity, (b) radial velocity, (c) axial heat flux, (d) radial heat flux, (e) temperature and (f) density

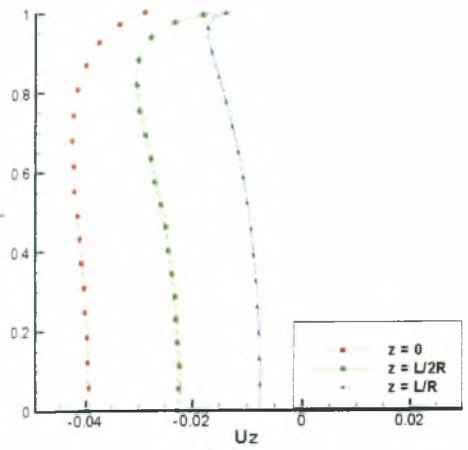

(a)

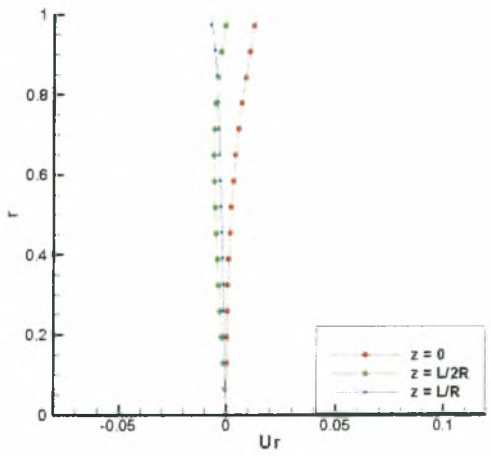

(b)

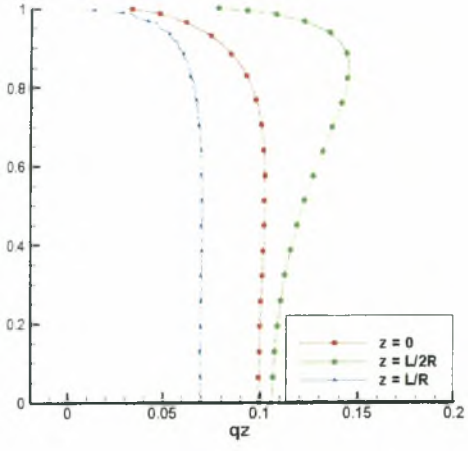

(c)

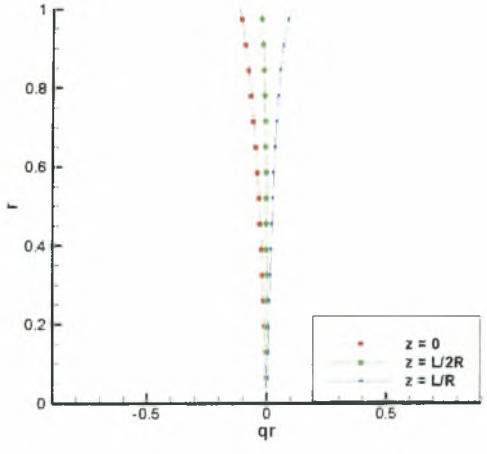

(d)

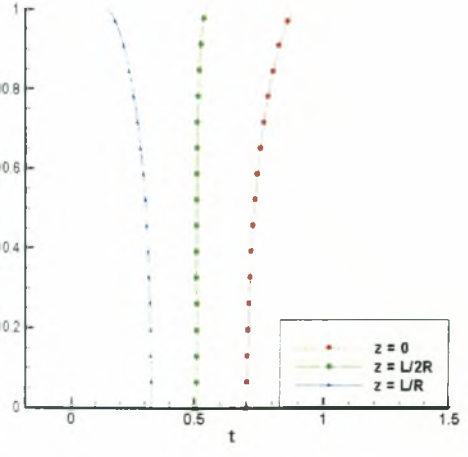

(e)

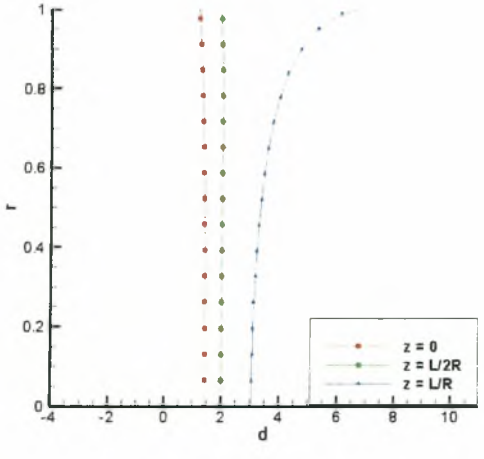

(f)

Figure 5.4: Macroscopic distributions along the tube with $L/R = 1$, $T_C/T_H = 0.1$ and δ=5.
(a) Axial velocity, (b) radial velocity, (c) axial heat flux, (d) radial heat flux, (e) temperature and (f) density

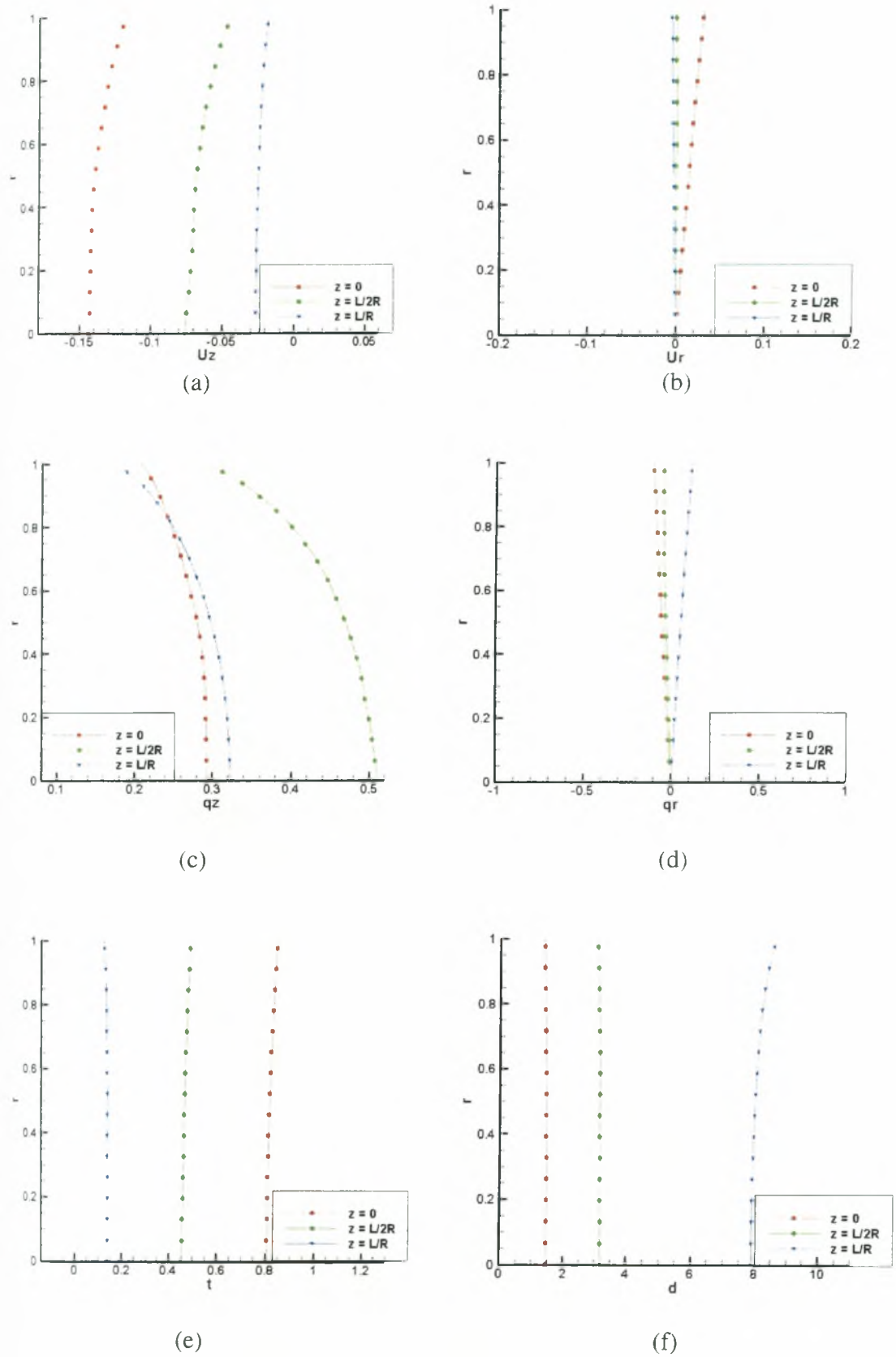

Figure 5.5: Macroscopic distributions along the tube with $L/R = 5$, $T_C/T_H = 0.1$ and $\delta = 0$.
(a) Axial velocity, (b) radial velocity, (c) axial heat flux, (d) radial heat flux, (e) temperature and (f) density

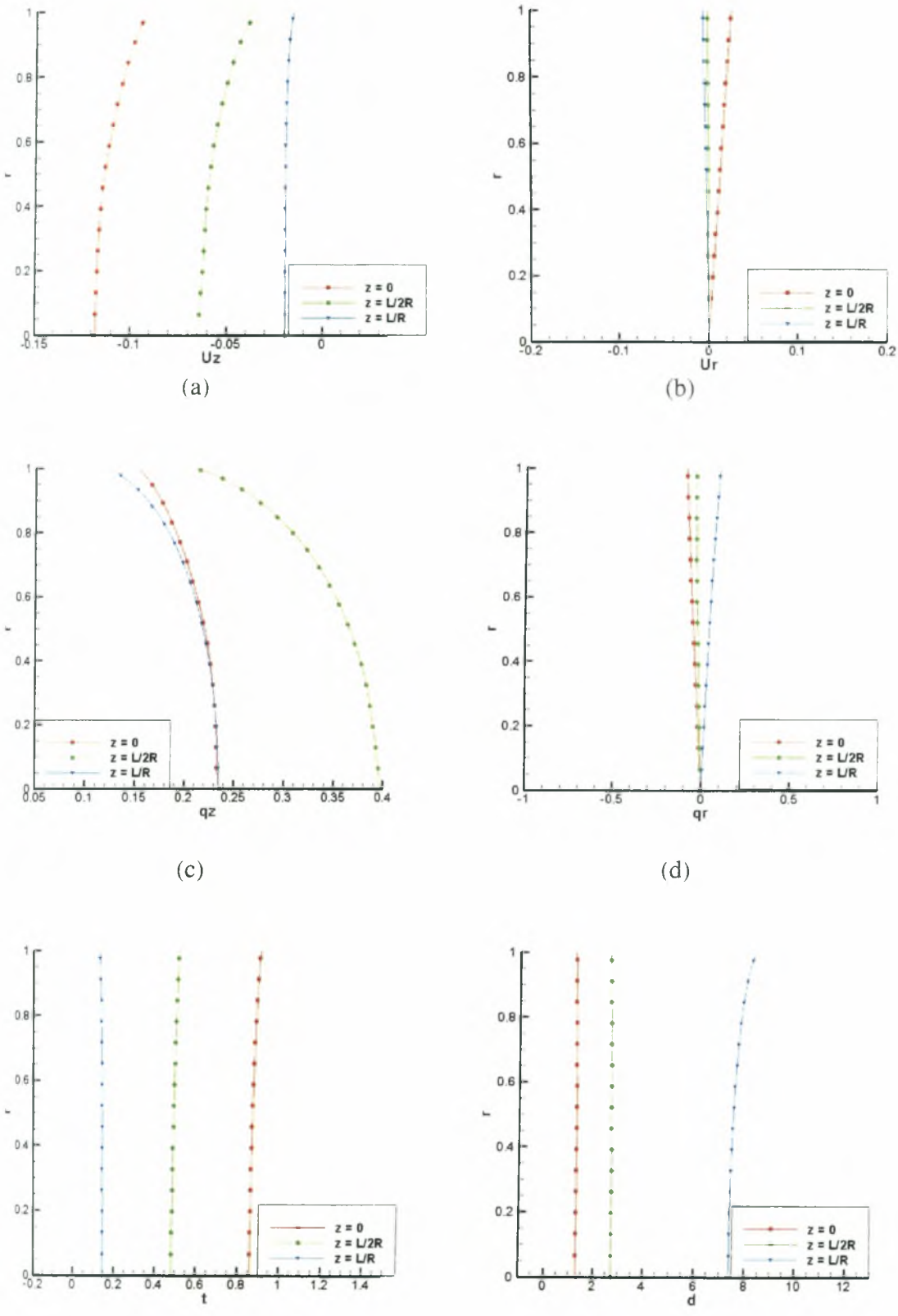

Figure 5.6: Macroscopic distributions along the tube with $L/R = 5$, $T_C/T_H = 0.1$ and $\delta = 0.1$.
(a) Axial velocity, (b) radial velocity, (c) axial heat flux, (d) radial heat flux, (e) temperature and (f) density

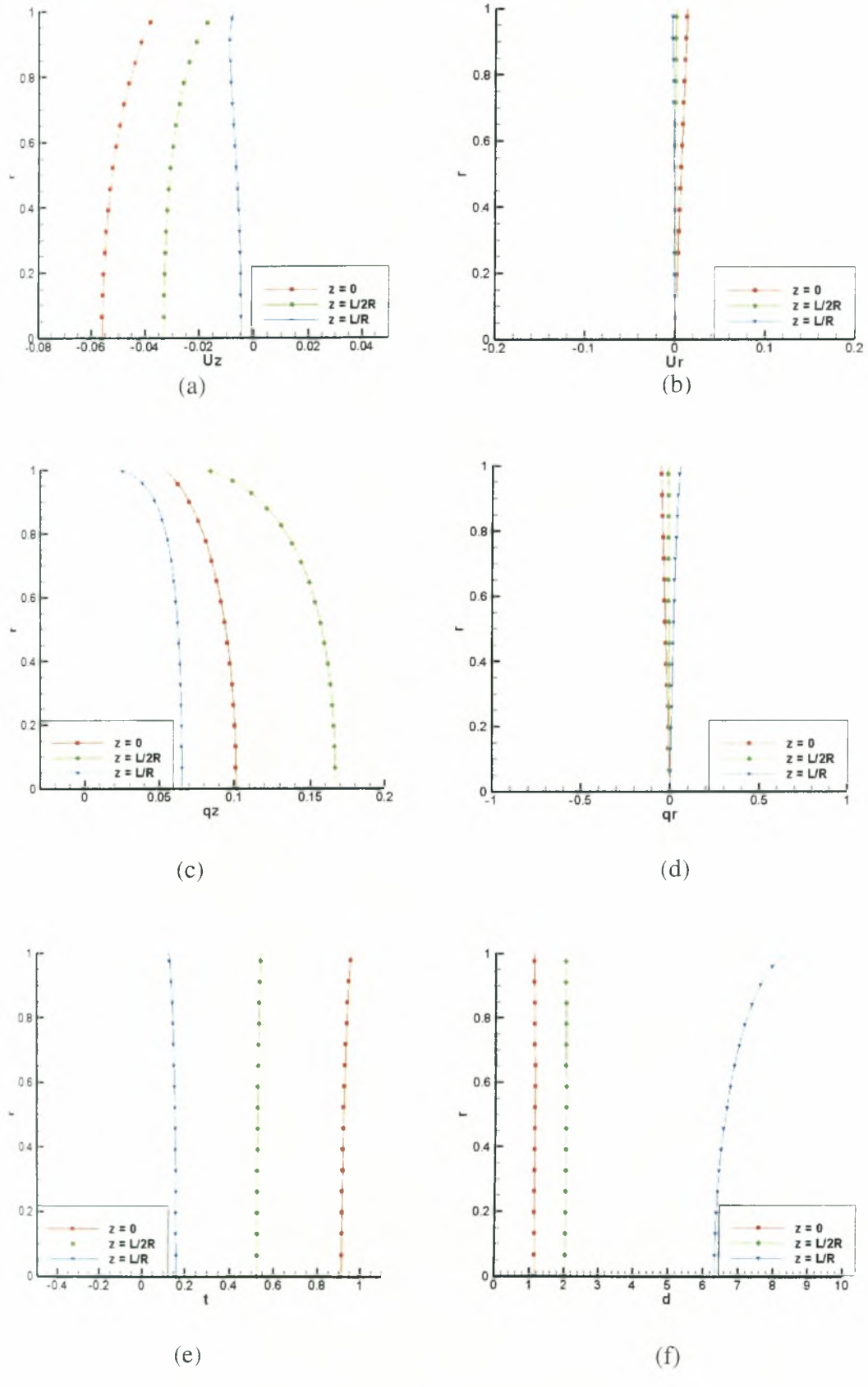

Figure 5.7: Macroscopic distributions along tube with $L/R = 5$, $T_C/T_H = 0.1$ and $\delta = 1$.
(a) Axial velocity, (b) radial velocity, (c) axial heat flux, (d) radial heat flux, (e) temperature and (f) density

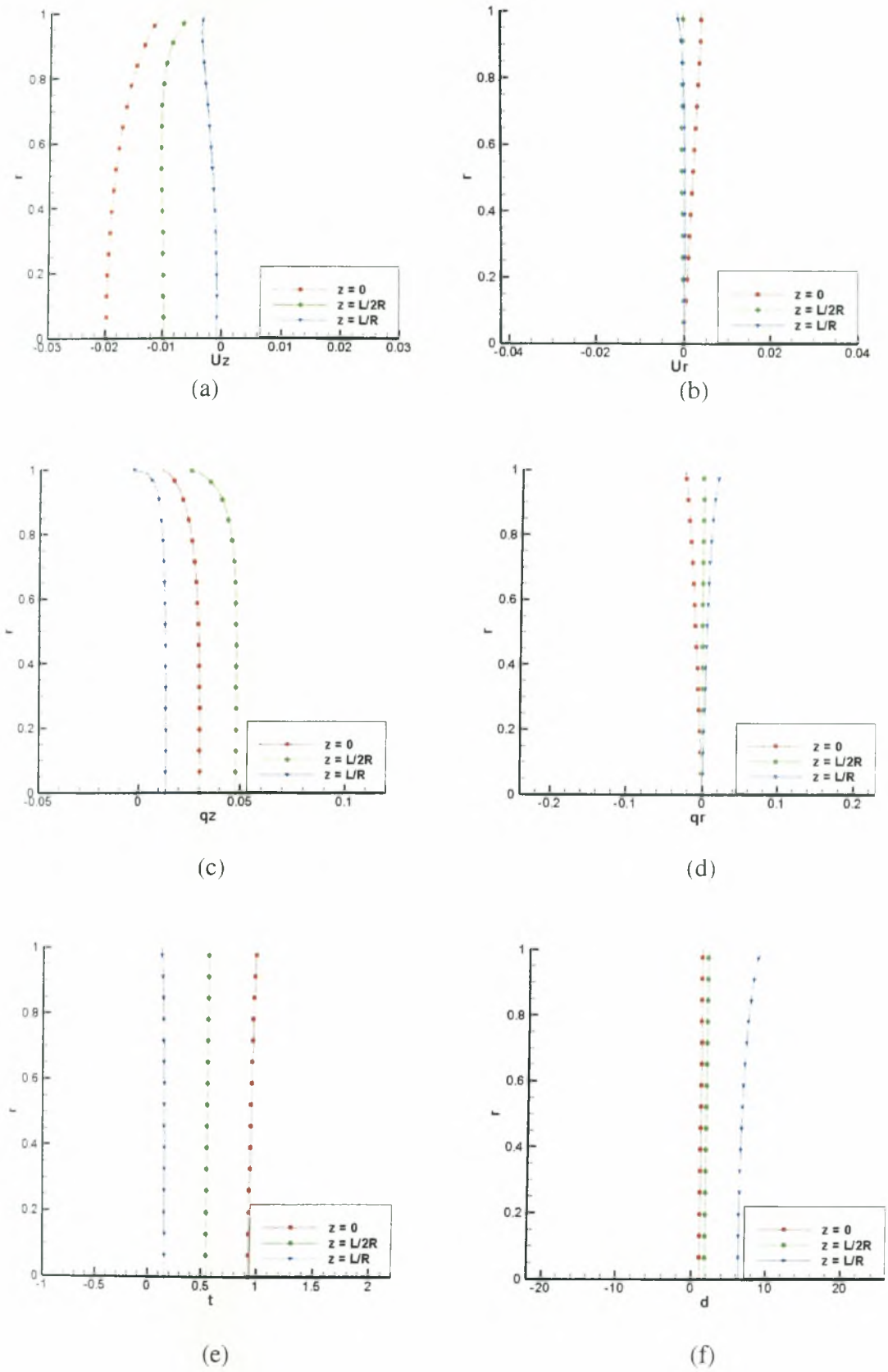

Figure 5.8: Macroscopic distributions along tube with $L/R = 5$, $T_C/T_H = 0.1$ and $\delta = 5$.
(a) Axial velocity, (b) radial velocity, (c) axial heat flux, (d) radial heat flux, (e) temperature and (f) density

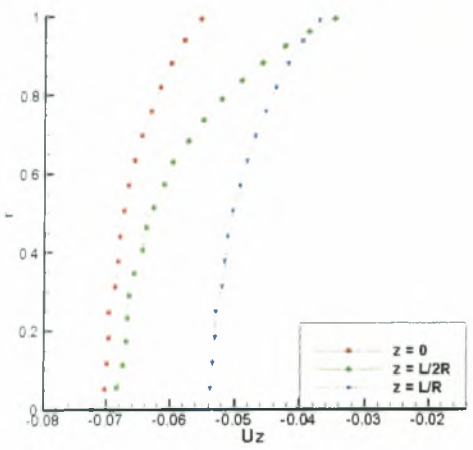

(a)

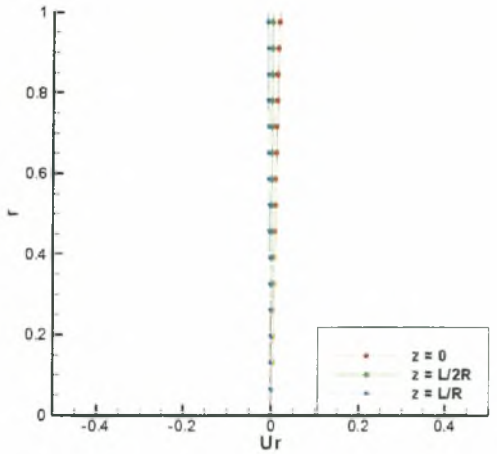

(b)

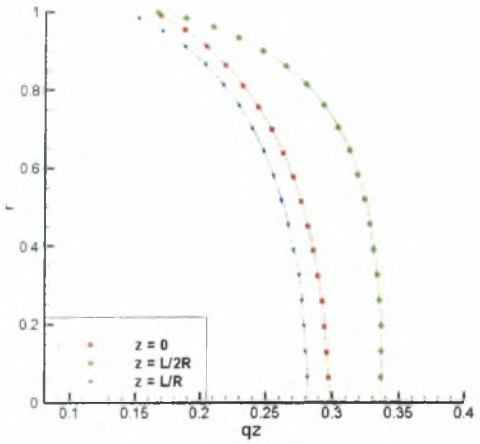

(c)

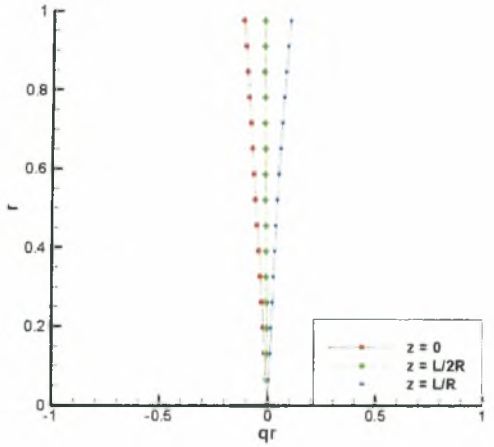

(d)

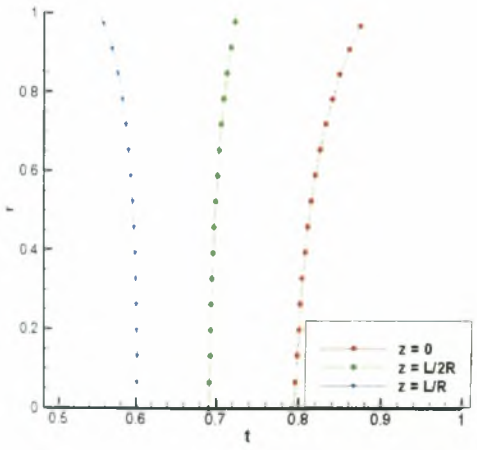

(e)

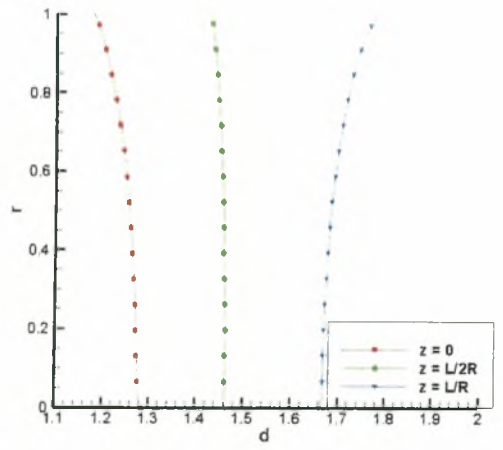

(f)

Figure 5.9: Macroscopic distributions along the tube with $L/R = 1$, $T_C/T_H = 0.5$ and $\delta = 0$.
(a) Axial velocity, (b) radial velocity, (c) axial heat flux, (d) radial heat flux, (e) temperature and (f) density

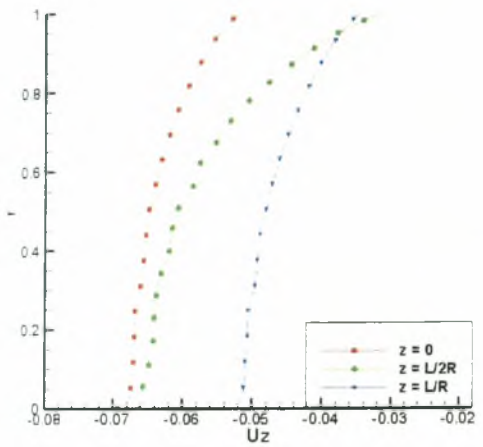

(a)

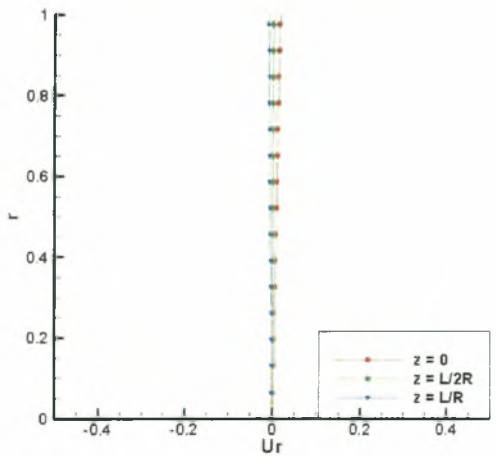

(b)

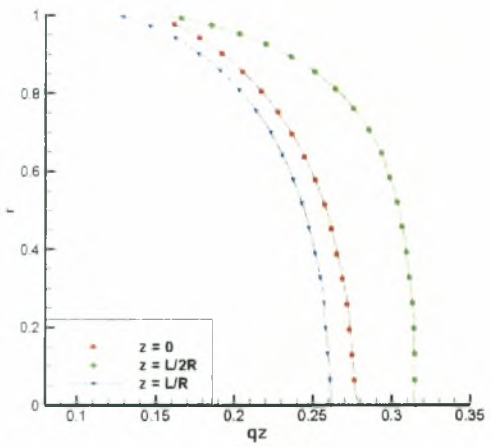

(c)

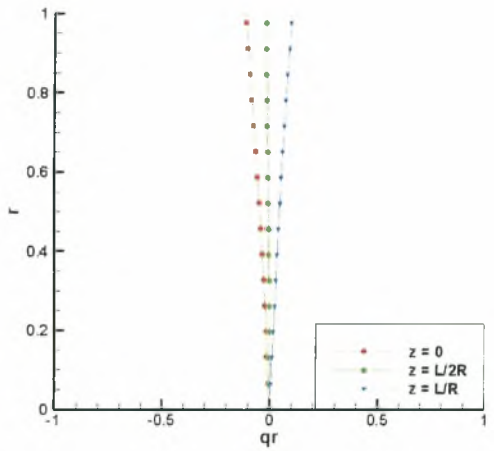

(d)

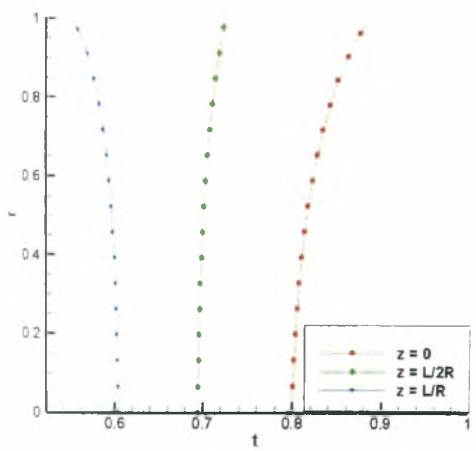

(e)

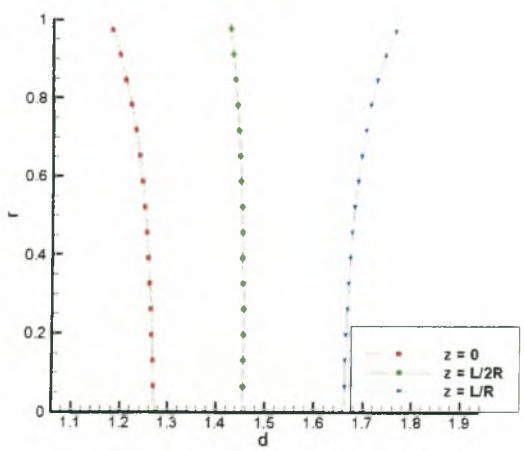

(f)

Figure 5.10: Macroscopic distributions along the tube with $L/R = 1$, $T_C/T_H = 0.5$ and $\delta = 0.1$.
(a) Axial velocity, (b) radial velocity, (c) axial heat flux, (d) radial heat flux, (e) temperature and (f) density

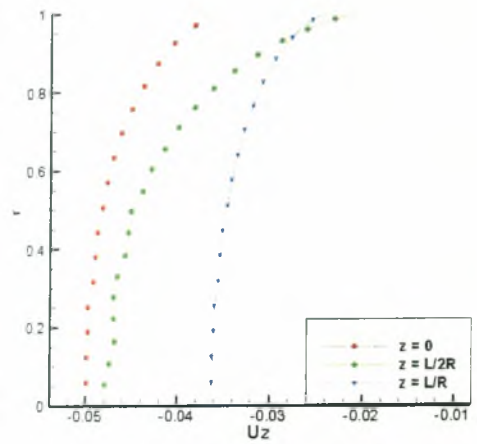

(a)

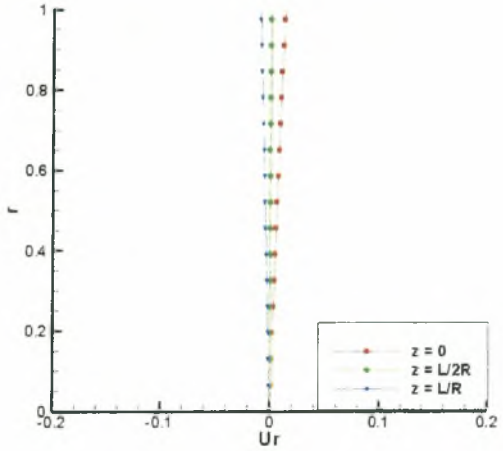

(b)

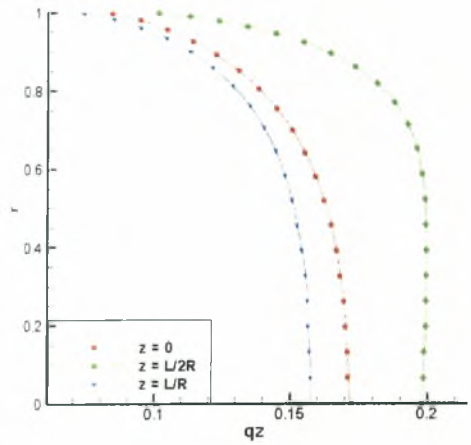

(c)

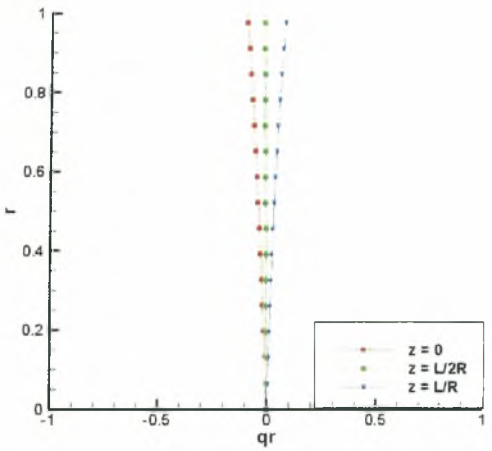

(d)

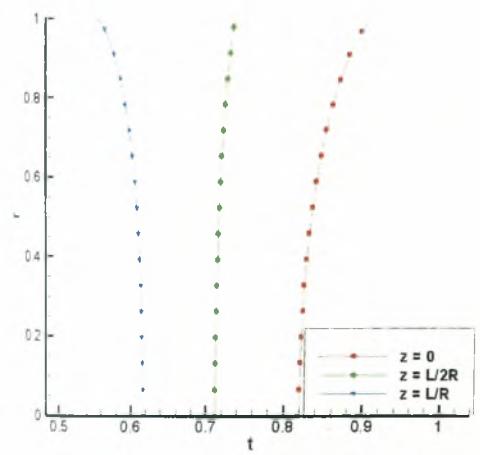

(e)

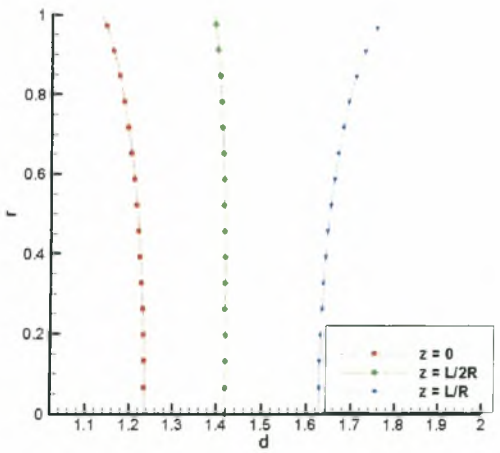

(f)

Figure 5.11: Macroscopic distributions along the tube with $L/R = 1$, $T_C/T_H = 0.5$ and $\delta = 1$.
(a) Axial velocity, (b) radial velocity, (c) axial heat flux, (d) radial heat flux, (e) temperature and (f) density

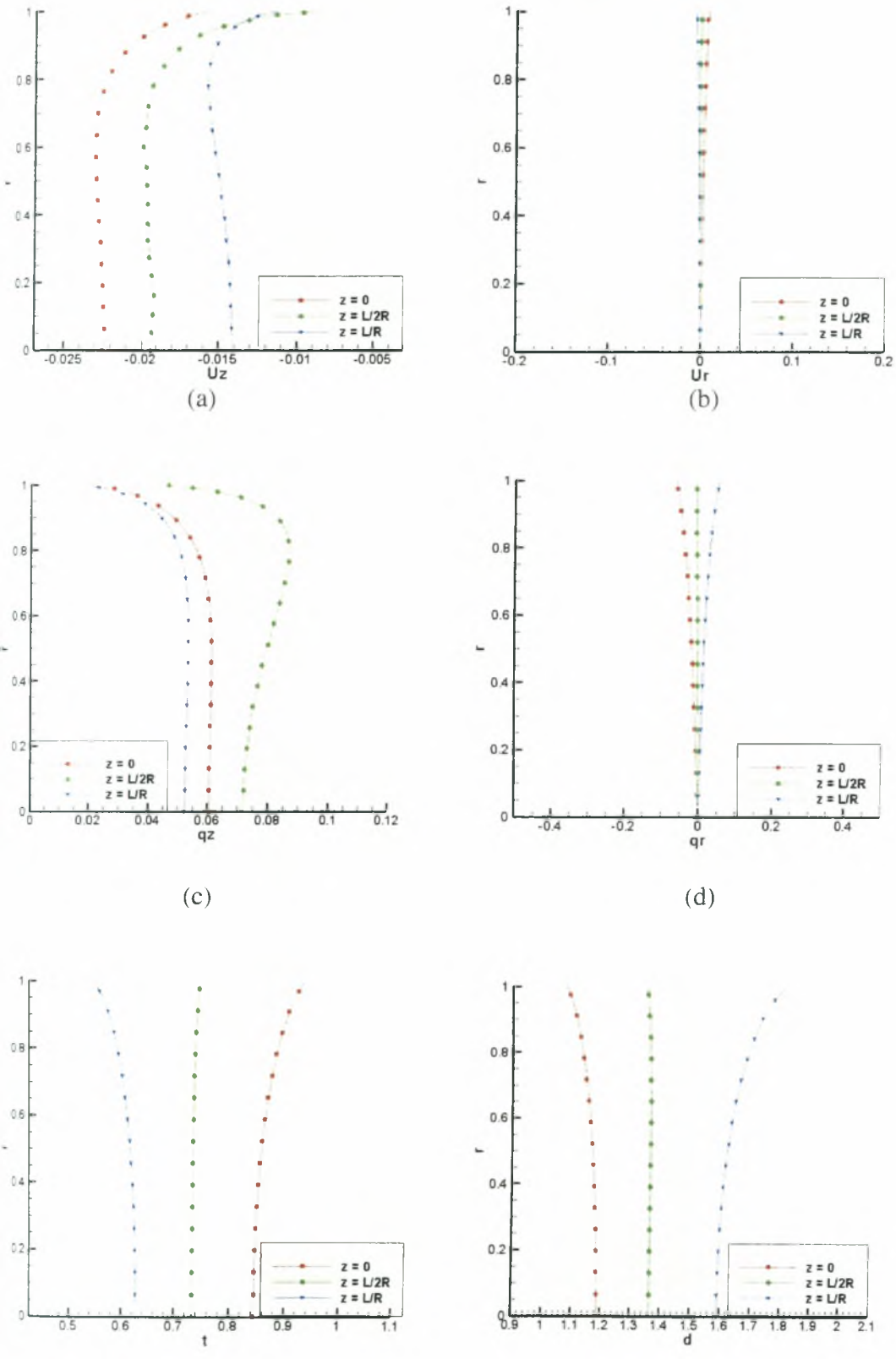

(a) (b)

(c) (d)

(e) (f)

Figure 5.12: Macroscopic distributions along the tube with $L/R = 1$, $T_C/T_H = 0.5$ and $\delta = 5$.
(a) Axial velocity, (b) radial velocity, (c) axial heat flux, (d) radial heat flux, (e) temperature and (f) density

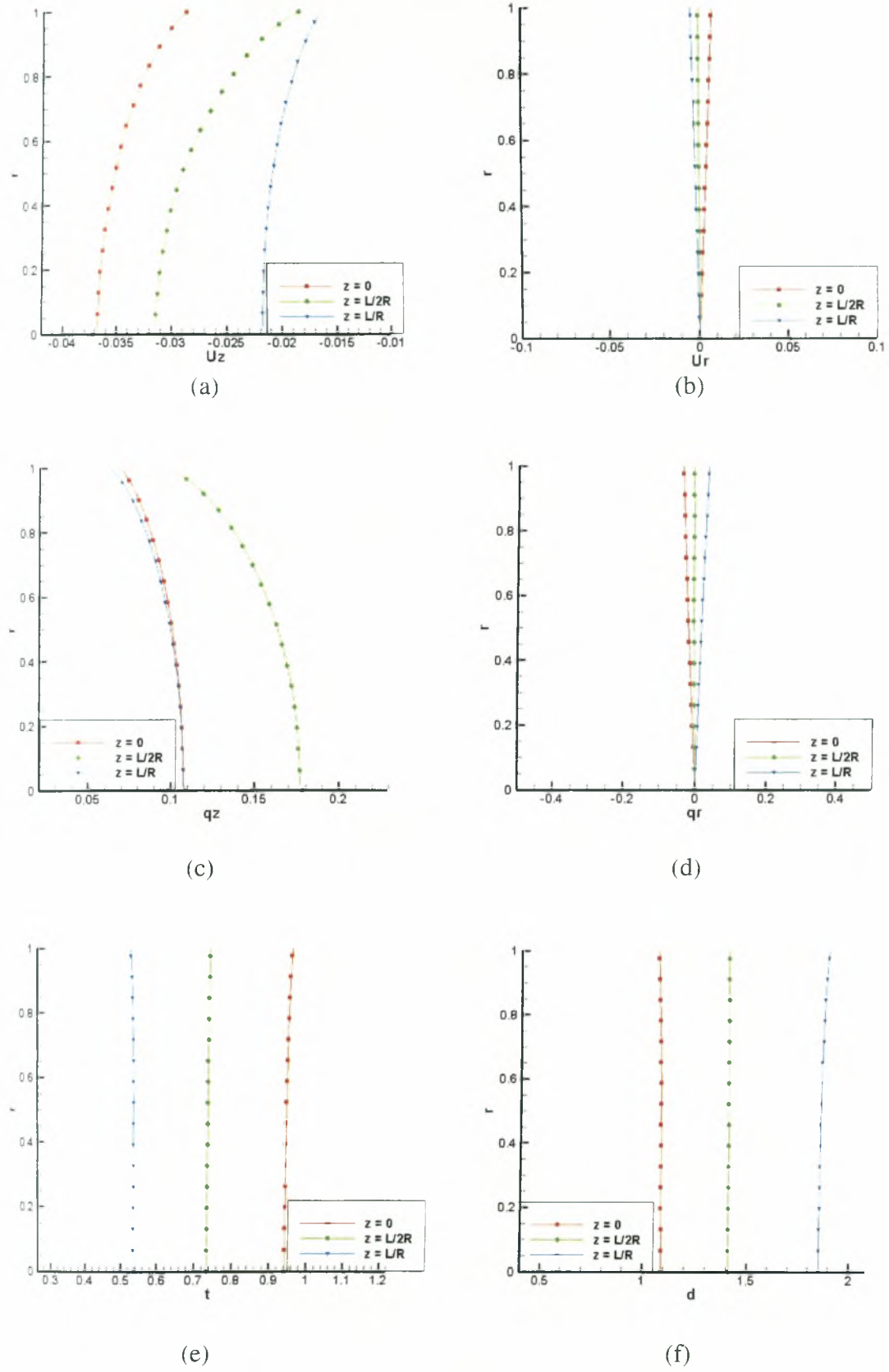

Figure 5.13: Macroscopic distributions along the tube with $L/R = 5$, $T_C/T_H = 0.5$ and $\delta = 0$.
(a) Axial velocity, (b) radial velocity, (c) axial heat flux, (d) radial heat flux, (e) temperature and (f) density

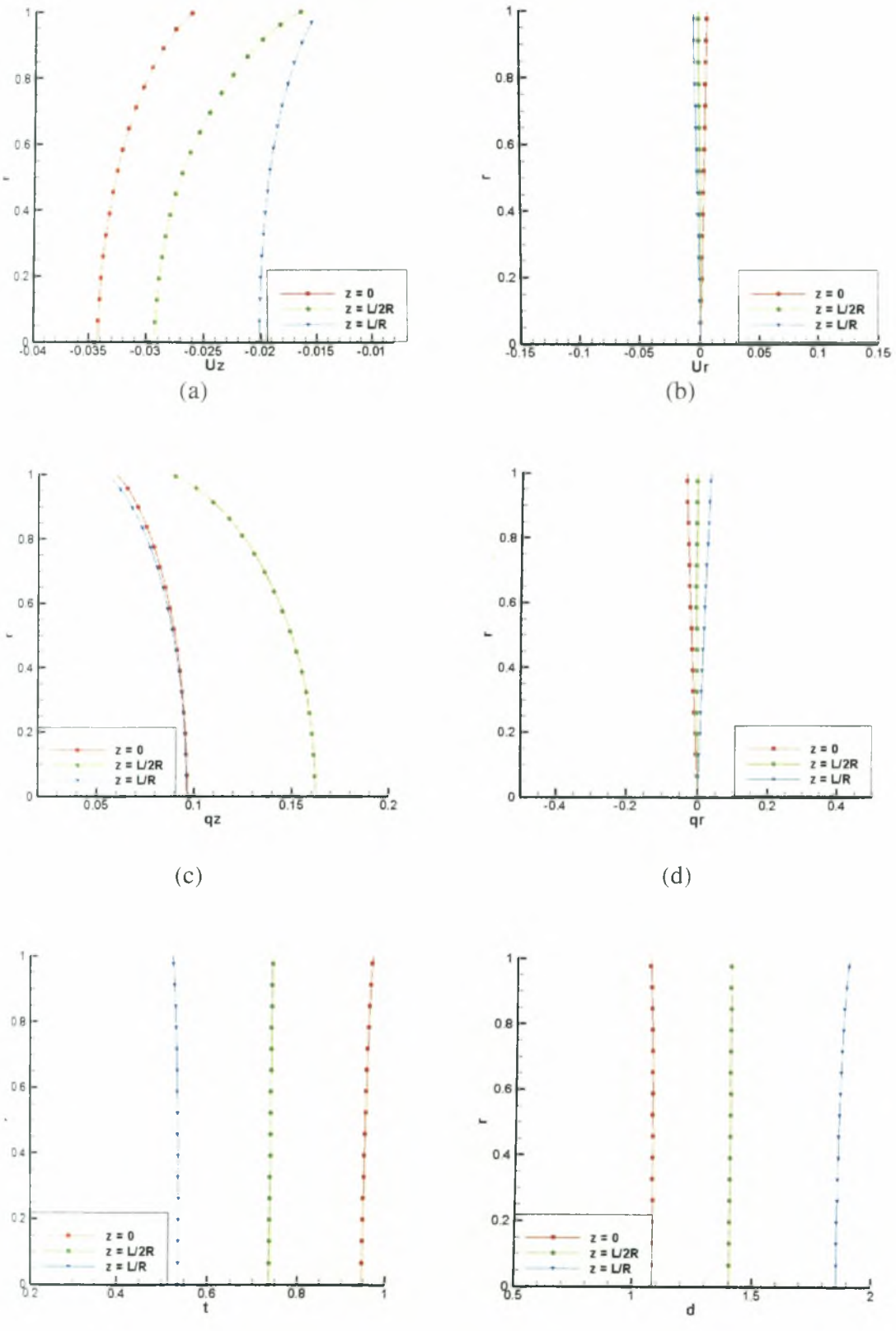

Figure 5.14: Macroscopic distributions along the tube with $L/R = 5$, $T_C/T_H = 0.5$ and $\delta = 0.1$.
(a) Axial velocity, (b) radial velocity, (c) axial heat flux, (d) radial heat flux, (e) temperature and (f) density

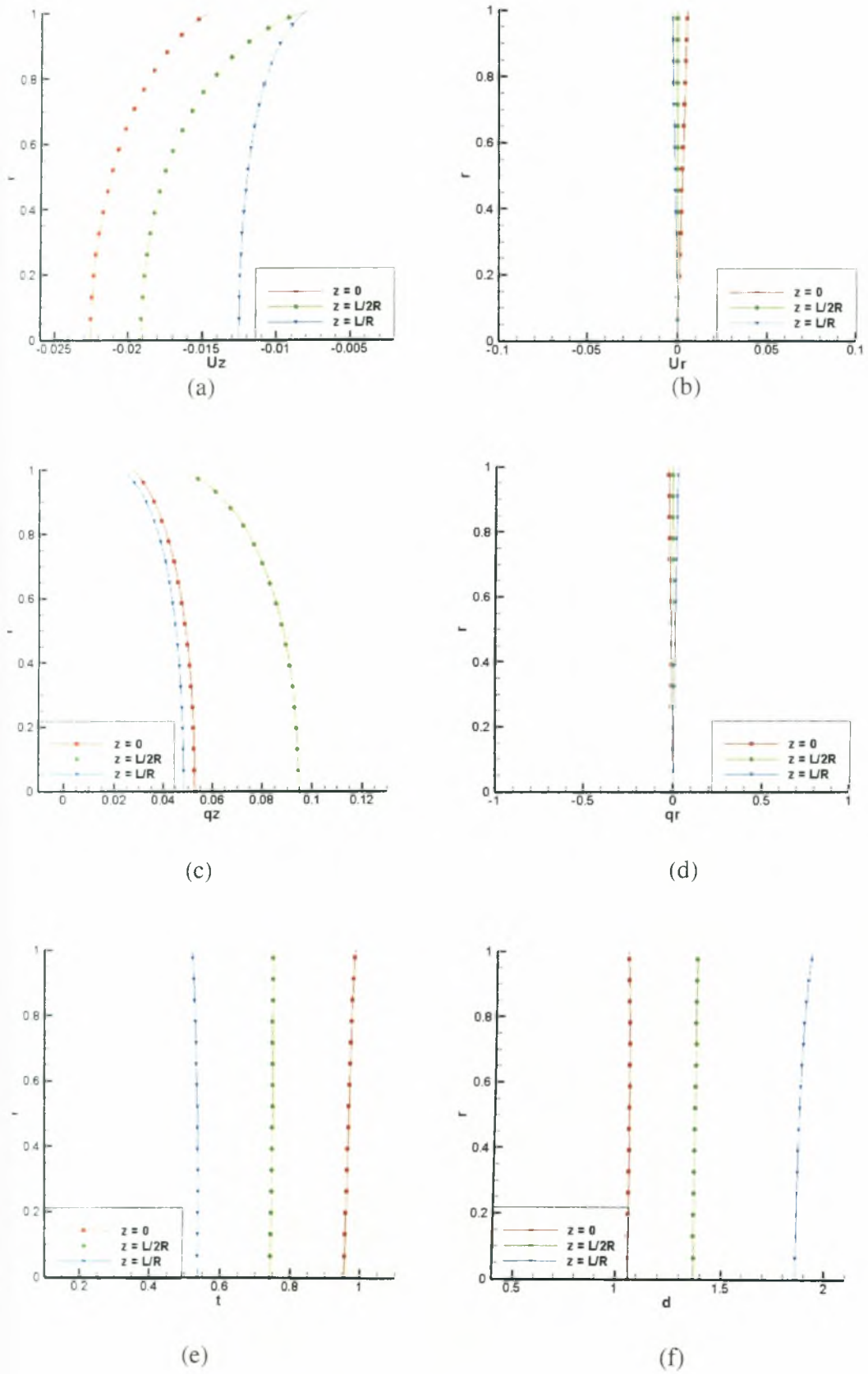

Figure 5.15: Macroscopic distributions along the tube with $L/R = 5$, $T_C/T_H = 0.5$ and $\delta = 1$.
(a) Axial velocity, (b) radial velocity, (c) axial heat flux, (d) radial heat flux, (e) temperature and (f) density

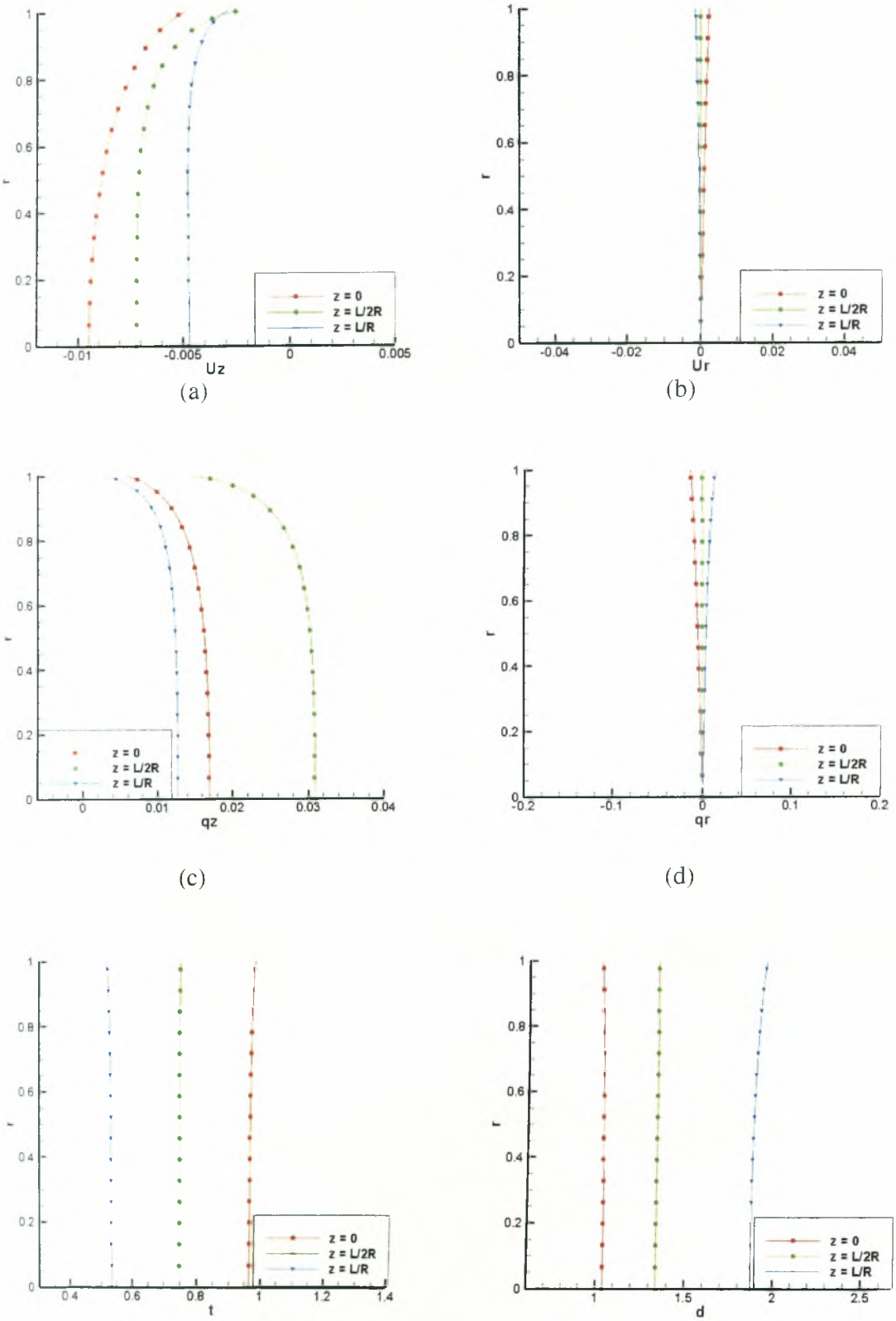

Figure 5.16: Macroscopic distributions along the tube with $L/R = 5$, $T_C/T_H = 0.5$ and $\delta = 5$.
(a) Axial velocity, (b) radial velocity, (c) axial heat flux, (d) radial heat flux, (e) temperature and (f) density

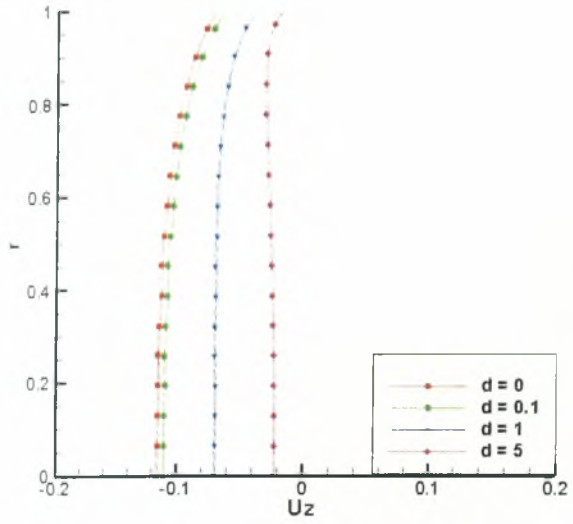

(a)

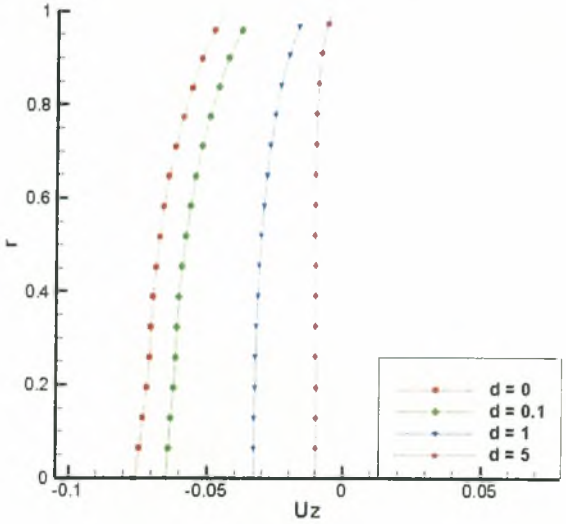

(b)

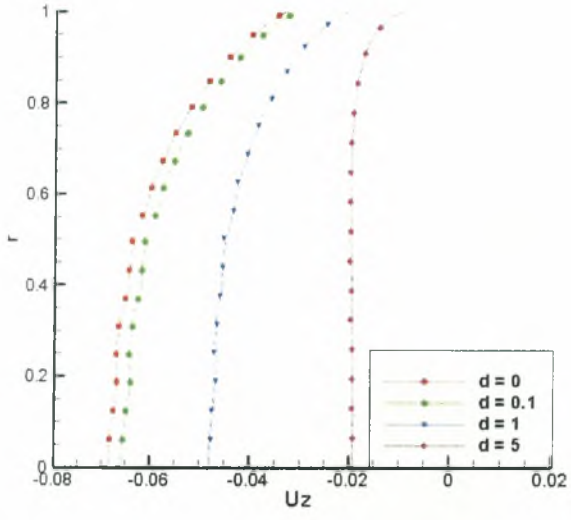

(c)

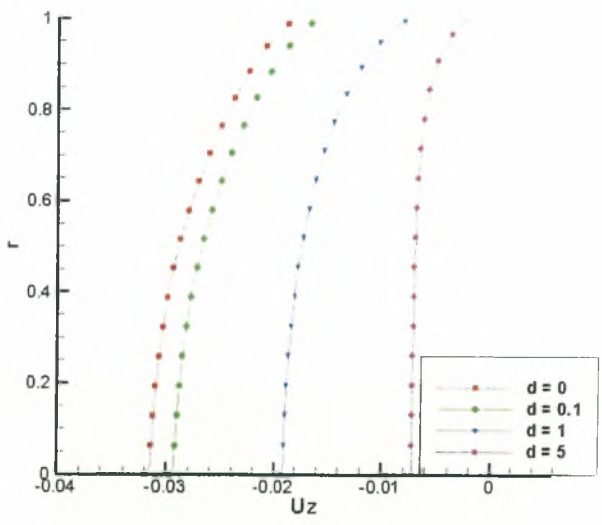

(d)

Figure 5.17: Distributions of axial velocity
(a) $L/R = 1$, $T_C/T_H = 0.1$, (b) $L/R = 5$, $T_C/T_H = 0.1$, (c) $L/R = 1$, $T_C/T_H = 0.5$ and (d) $L/R = 5$, $T_C/T_H = 0.5$

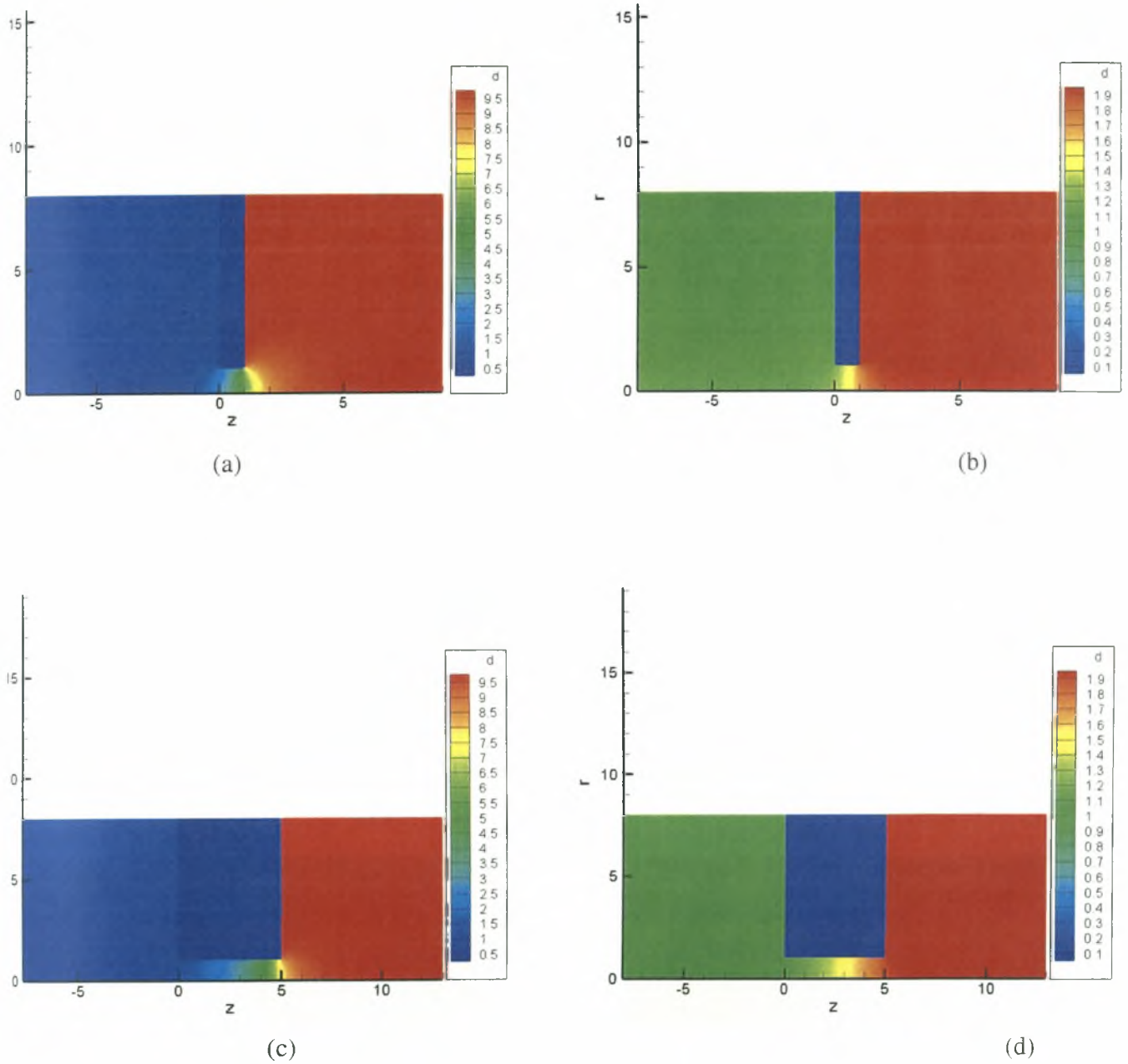

Figure 5.18: Density distributions for the tube geometry with $\delta = 0.1$
(a) $L/R = 1$, $T_C/T_H = 0.1$, (b) $L/R = 1$, $T_C/T_H = 0.5$, (c) $L/R = 5$, $T_C/T_H = 0.1$ and (d) $L/R = 5$, $T_C/T_H = 0.5$

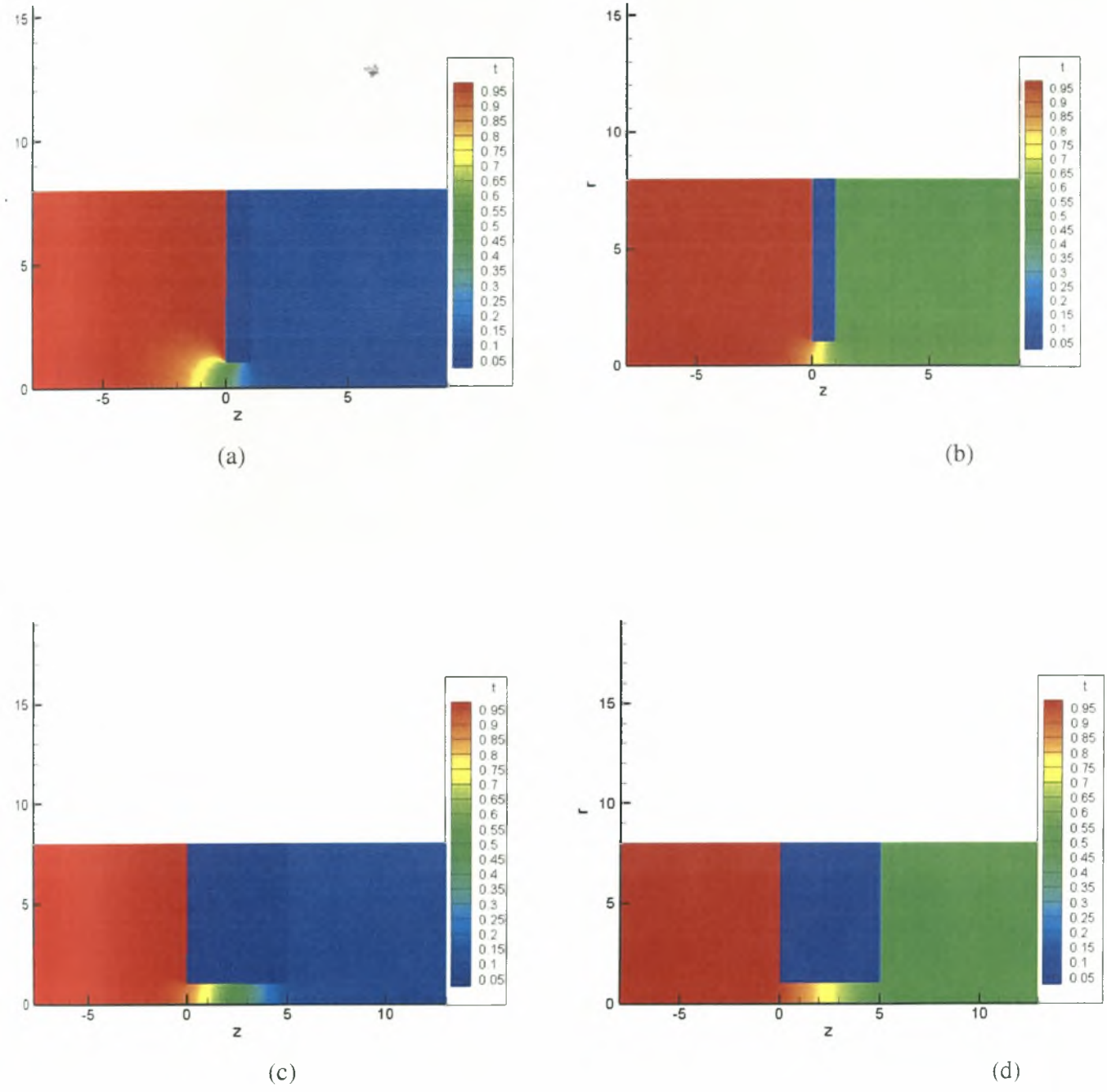

Figure 5.19: Temperature distributions for the tube geometry with $\delta = 0.1$
(a) $L/R = 1$, $T_C/T_H = 0.1$, (b) $L/R = 1$, $T_C/T_H = 0.5$, (c) $L/R = 5$, $T_C/T_H = 0.1$ and (d) $L/R = 5$, $T_C/T_H = 0.5$

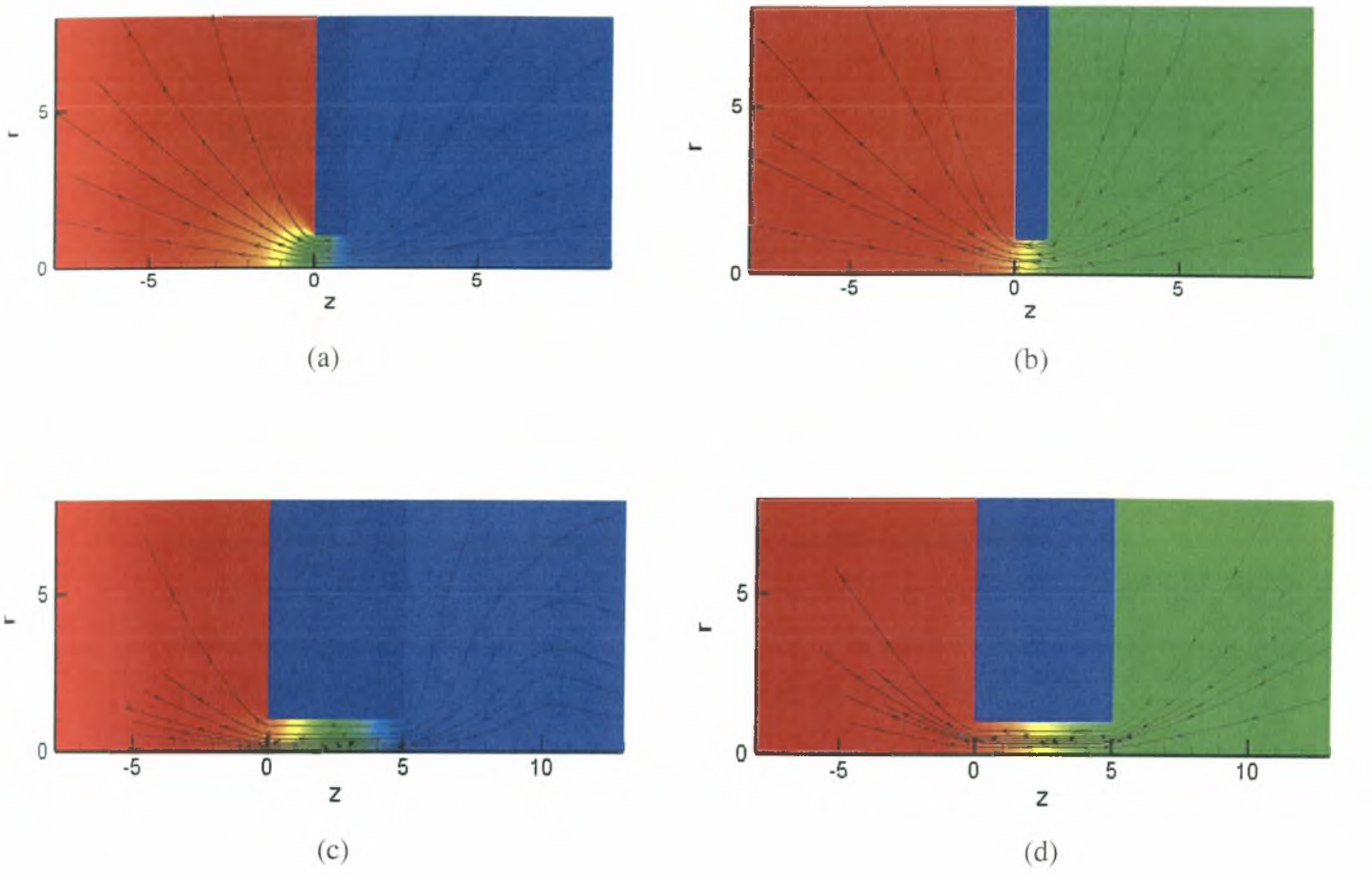

Figure 5.20: Streamlines for the tube geometry with $\delta = 0.1$
(a) $L/R = 1$, $T_C/T_H = 0.1$, (b) $L/R = 1$, $T_C/T_H = 0.5$, (c) $L/R = 5$, $T_C/T_H = 0.1$ and (d) $L/R = 5$, $T_C/T_H = 0.5$

Chapter 6

Knudsen pumps

6.1 Fabricated thermal transpiration pumps

6.1.1 The Knudsen compressor

A Knudsen compressor generates large changes in pressure by utilizing a cascade of multiple stages. Each stage is composed of a capillary and connector section. A temperature increase across the capillaries results in a thermal transpiration driven, pressure increase. The capillary section is followed by a connector section where the pressure is approximately constant, while the temperature drops to its original value entering the stage. Figure 6.1 outlines an illustrative single stage of a Knudsen compressor.

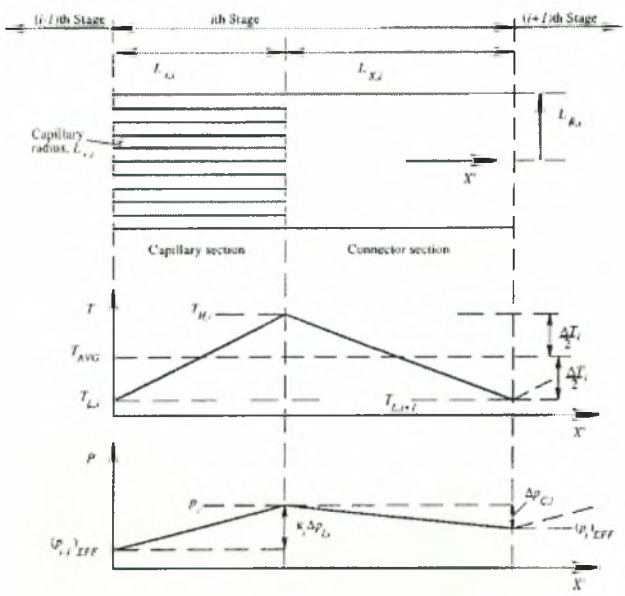

Figure 6.1: Illustrative single stage of a Knudsen compressor (Vargo et. Al, 1999)

The original analysis of a Knudsen compressor's performance was based on the assumption of an ideal situation of free – molecule flow in the capillary section and continuum flow in the connector section of a compressor stage. While these conditions can be closely matched in laboratory compressors, it is expected in practice that both the capillary and the connector sections of the compressor frequently will operate in the transitional flow regime [Vargo et al., 1999].

6.1.2 Micromachine based vacuum pump on a chip actuated by the thermal transpiration effect

As it was previously mentioned, gas micropumping technology takes interest in many applications, ranging from portable handheld gas sensing microsystems such as breath analyzers, to filtration and by – pass medical devices [Gupta & Gianchandani, 2008, Pharas & McNamara, 2010].

As mentioned before, a major challenge in the design of a thermal transpiration based pumps is to ensure good thermal isolation between the hot and cold ends of the pump to maximize the thermal difference. The primary parameters affecting the thermal isolation are the thermal conductivity of the pump channel material, and the length of the channel separating the hot and the cold sides. Typically, a Knudsen pump uses a resistive heater to actively heat the hot side and the cold side is passively cooled as shown in Figure 6.2.

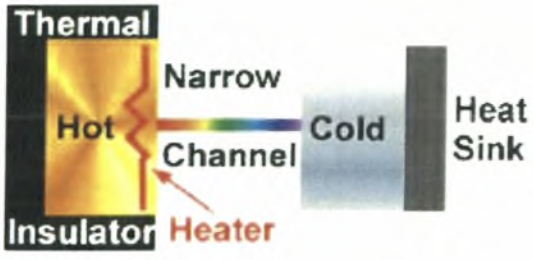

Figure 6.2: A conventional Knudsen pump utilizing a resistive heater has an asymmetric design (Pharas and McNamara, 2010)

The total power consumption is minimized by thermally insulating the hot side. This creates an asymmetric design in which the hot and the cold sides have different geometries and different material requirements [Pharas & McNamara, 2010].

A novel technique to create a vacuum pump on an integrated circuit chip was presented by R. M. Young. It must be noted that, thermal transpiration pumps are particularly suited to miniaturization and fabrication by integrated circuit (IC) lithographic techniques. The pump proposed by Young consists of small tubes, operating in the free molecular flow regime, connected to larger, although still miniature, flow chambers. The gas is alternately heated and cooled as it traverses these tubes and chambers, the thermal transpiration effect creating a mass flow and compression in each stage. The pump has no moving parts, eliminating wear and particulate generation and increasing reliability. Also, the power is low, in the milliwatt range, permitting battery power for portability; no valves are required and the pump is silent, with no noise being generated.

The thermal transpiration effect has been used in the measurement of thermodynamic and transport properties of gases. Also, the thermal transpiration effect can be used to construct a dynamic, i.e. continuously flowing, vacuum pump, as demonstrated by a number of researchers over the years. All of these previous pumps have been large, macroscopic benchtop or larger units, and have been laboriously fashioned. Machining the critical dimension $R << \lambda$ is technically quite challenging using conventional fabrication techniques. Muntz et al. have demonstrated in a laboratory unit that a micromachined membrane of microchannels can be successfully used to create a thermal transpiration vacuum pump.

The characteristic etch depth and thin film deposition thicknesses used in IC fabrication are typically of the order of the mean free path length (about 65nm for room temperature air at atmospheric pressure). Thus, as pointed out by several researchers, there is a natural coincidence in MEMS fabrication technology and pump dimensions for thermal transpiration pumps. Figure 6.3 shows a top view schematic of a chip which has been etched to form a series of free molecular flow tubes connecting larger, continuum flow chambers.

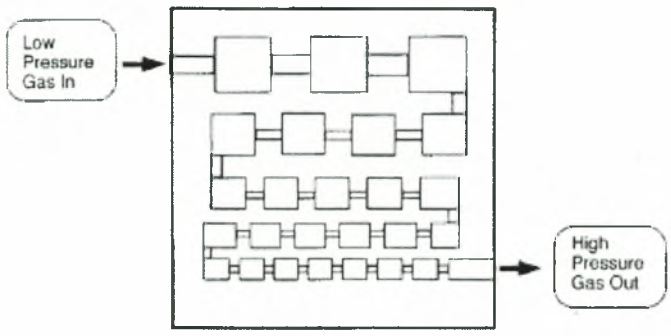

Figure 6.3: Top view schematic of a MEMS fabricated, multistage thermal transpiration pump on a chip (Young, 1999)

Since each stage is limited in compression ratio by, at best, the square root of the temperature ratio, multiple stages are required. One manufacturing advantage now gained is ease of fabrication of these many stages for, IC MEMS photolithography permits fabrication of many chambers and tubes just as IC lithography permits the fabrication of many transistors on a chip.

At one end of the connecting tube, the gas must be heated for the pumping to take place. Thin film heaters, fabricated on the substrate, are simple and robust. From a heat transfer point of view, placing the heater in direct contact with the substrate heats mostly the substrate. Only a small portion of the power ends up in the gas, and indeed, one only needs to heat up the gas. Heating the substrate results in wasted power. Thus, placing the heater on an air bridge, shown in Figure 6.4, reduces power consumption by an order of magnitude.

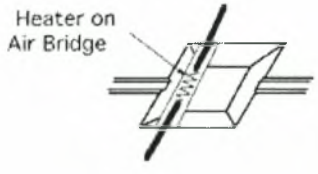

Figure 6.4: Three –dimensional scheme of a MEMS fabricated thermal transpiration pump cell, showing an air bridge heater located at the left end of the large continuum cell, and two connecting tubes, whose length is small in comparison with the mean free path length (Young, 1999)

Micromachined air bridge heaters have been demonstrated to be low power, typically 10–100 mW in atmospheric pressure air and lower in power in vacuum, and can

operate for indefinitely long periods of time at temperatures of 300 - 350 °C in atmospheric pressure air, and also readily reach 500 - 600 °C. They have even been demonstrated up to incandescence in air for short periods of time ~*T*51000 - 1400 K. With a proper encapsulant such as silicon nitride or oxide, they are potentially operational in corrosive atmospheres. Also, due to the physics of the thermal transpiration effect, lighter gases such as H_2 and He are pumped better than the heavier species; again this is an advantage over many other types of pumps.

The mass flow throughout a round tube is limited, but obviously numerous such tubes, placed in parallel, can be formed to connect the two continuum cavities. Indeed, the free molecular tubes shown in Figure 6.4 are roughly rectangular in cross section. The use of rectangular features is another advantage of using IC MEMS fabrication technology. The Knudsen criterion for free molecular flow is based on the shallowest dimension, in our case the depth characteristic length of such a rectangle. It is very easy for us to pattern these tubes and etch them to depths ranging from the submicron up to hundreds of microns. The cross-sectional scheme shown in Figure 6.5 illustrates two stages of this pump, made up of two etched chips bonded together.

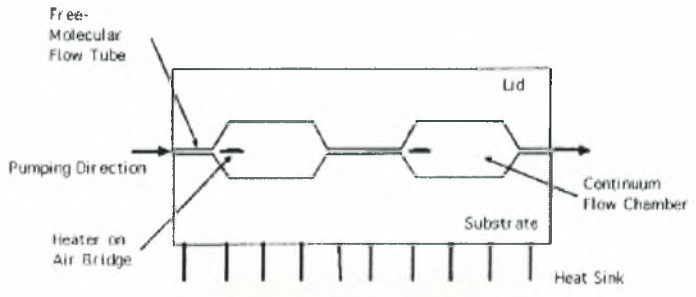

Figure 6.5: Cross – sectional schematic of the MEMS fabricated thermal transpiration pump (Young, 1999)

The pump is a dry pump, that is, no oil is used, either for lubrication and seals as in a piston pump, or as the working fluid as in a diffusion pump. This eliminates the need for cold traps to prevent oil from backstreaming into the sensor or other components, and there is no concern about oil aging or reacting with the gases being pumped. Being a dry pump also means that the pump will operate in any orientation.

This pump does not need valves to operate. Many other pumps require either passive or active valving to accomplish their compression (e.g., piston pumps). This

again increases reliability. Furthermore, it eliminates pulsations in the gas pressure or flow. It also makes the pump silent.

With proper engineering, this thermal transpiration pump on a chip can be self-priming, that is, it will pump from below 10 mTorr up to atmospheric pressure on its own; no fore pump is needed [Young, 1999].

6.1.3 Bidirectional operation of a gas pump

A novel solution to attaining a large thermal difference was presented by Pharas and McNamara. They first used a thermoelectric material in the bidirectional operation of a gas pump using thermal transpiration. The thermoelectric material maintains a higher temperature difference which favours thermal transpiration and thus increases the efficiency of gas pumping.

A thermoelectric module is used to actively heat the hot side, while simultaneously actively cooling the cold side. Without the need for a heat sink, the design is inherently symmetrical, as seen in Figure 6.6, and the pump can be operated in the forward or reverse directions by changing the direction of current flow in the thermoelectric module, making this design the first bidirectional Knudsen pump.

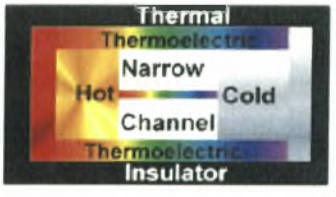

Figure 6.6: Knudsen pump using the thermoelectric module has a symmetric design (Pharas and McNamara. 2010)

Pharas and McNamara reported two experimental designs based on the use of the thermoelectric module.

The first design uses a long channel length to provide better thermal isolation between the hot and cold sides, while the second design uses a short channel length to minimize the gas flow impedance through the channel and improve the gas flow rate.

The schemes of the two Knudsen pump designs are shown in Figure 6.7, below.

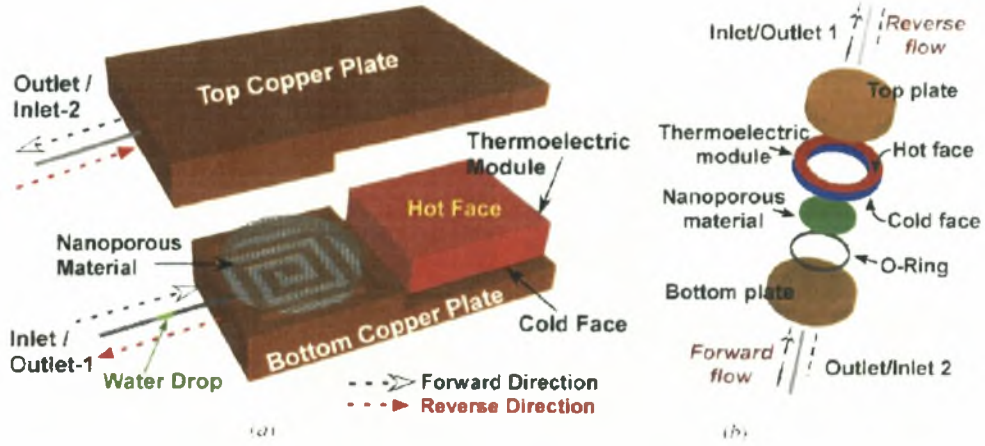

Figure 6.7: (a) Scheme of the bidirectional Knudsen pump using the lateral design and (b) Exploded view of the bidirectional Knudsen pump using the radial design (Pharas and McNamara, 2010)

In Figure 6.7(a), a thermoelectric module is thermally coupled to a nanoporous material with the use of a top and a bottom copper plate. The temperature difference across the nanoporous material causes a gas flow due to thermal transpiration. An inlet and outlet are formed on either side of the nanoporous material. This design is referred to as the lateral pump design.

In Figure 6.7(b), a thermoelectric module in the shape of a ring is thermally coupled to a nanoporous material with the use of a top and bottom plate. This design is referred to as the radial pump design. For both designs when the thermoelectric is powered on, one face gets hotter while the other face gets colder. The plates serve as heat spreaders to transfer thermal energy from both faces of the thermoelectric module to either side of the nanoporous material, and thus control the hot and cold end temperatures of the channels.

Gas is pumped from the cold side inlet to the hot side outlet due to thermal transpiration. For a 100nm pore size channel over a temperature range of 280 – 380K, Kn is between 0.53 and 0.72, while for a 50nm pore size channel over the same range of temperature, Kn is between 1.07 and 1.45. Thus, all the experiments were conducted in the transition flow regime. Insulating the pump with a low thermally conductive material will help lower the heat losses to the environment. The radial

pump design has no thermal insulation and the lateral pump design has plastic sheets that help insulate it.

Photographs of the fabricated devices are shown in Figure 6.8. Each device has two thermocouples embedded in them, one for the hot side and one for the cold side.

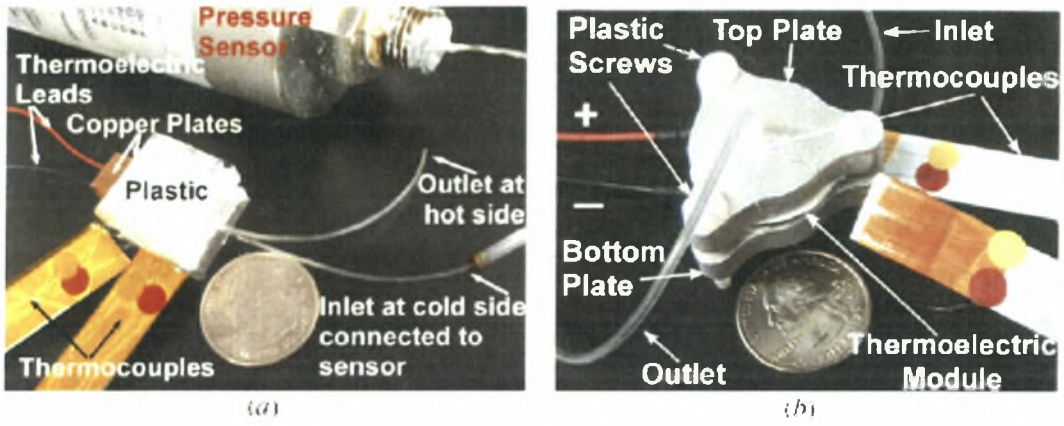

Figure 6.7: Photographs of the actual pumps: (a) lateral pump design and (b) radial pump design (Pharas and McNamara, 2010)

After simulations of the devices, Pharas and McNamara showed that the radial pump design achieved a normalized flow rate that is 50 times greater than the lateral pump design. The reason for this improved flow rate include a higher temperature difference across the nanoporous material, a more uniform temperature distribution, and a thinner nanoporous material that permits a higher flow rate. The pump works in both directions, with a lower flow rate in the reverse direction [Pharas & McNamara, 2010].

6.1.4 Thermal transpiration in zeolites

Although the phenomenon of thermal transpiration has been known for more than a century, very few efforts have focused on the atmospheric pressure operation of a Knudsen pump because this requires channels with hydraulic diameter smaller than approximately 100 nm. Vargo and Muntz reported a mesoscale device for operation near atmospheric pressure using nanoporous aerogel, providing a best case pressure

drop of 11.5 Torr (≈1.5 kPa) using helium. McNamara and Gianchandani reported the feasibility of using lithographically patterned nanochannels in a chipscale, fully micromachined, Knudsen pump that achieved a pressure drop of about 54.7 kPa with 80 mW of input power. However, the limitation on the density of lithographically patterned narrow channels in a micromachined Knudsen pump constrains the flow rate to the order of 10–6 cc/min [Gupta and Gianchandani, 2008].

In their 2008 work, Gupta and Gianchandani [Gupta and Gianchandani, 2008] explored the use of a naturally occurring zeolite, clinoptilolite, for a chip-scale, thermal transpiration-based gas pump.

Naturally occurring zeolites have a dense interconnected network of nanochannels (>10^{14} pores/cm^2). These billions of nanochannels can transpire gas in unison, resulting in gas flow rates significantly greater than possible with a micro-fabricated Knudsen pump having a limited number of lithographically patterned nanochannels. Clinoptilolite, the zeolite used in this study, is one of the most abundant and widely mined natural zeolites, and is easily machinable.

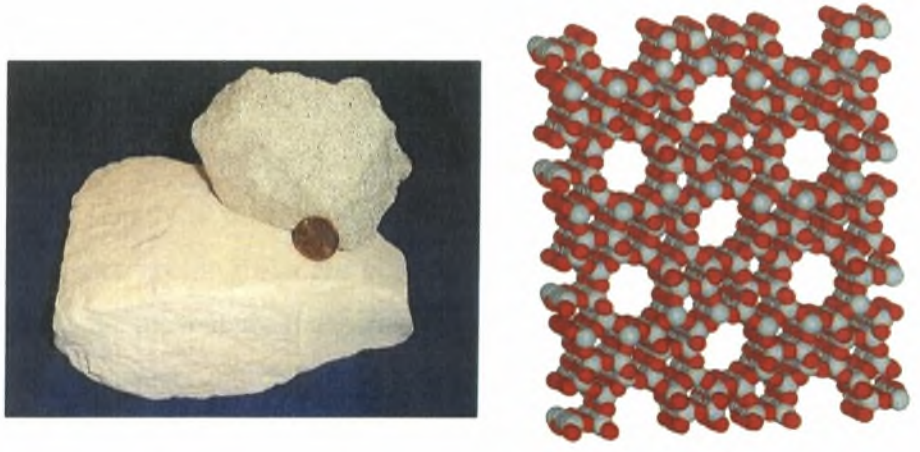

Figure 6.8: Crystal structure of Clinoptilolite

It has nanopores with hydraulic diameter of ≈0.45 nm and has bulk porosity of ≈34%, which enable the required free-molecular flow, even at atmospheric pressure. It is an inexpensive, easily accessible, and mechanically strong nanoporous material.

The zeolite-based Knudsen pump described here has two circular zeolite disks with a flexible heater sandwiched between them as shown in Figure 6.9 below:

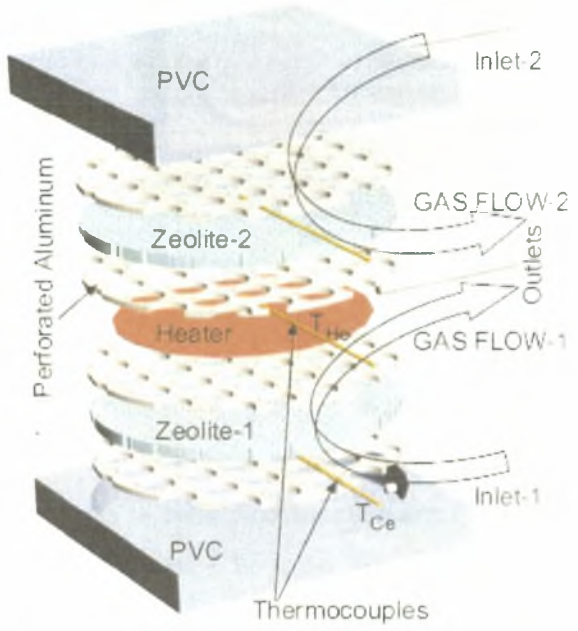

Figure 6.9: Exploded view of a zeolite-based Knudsen pump showing relative location of various components. The arrows represent the flow of pumped gas (Gupta and Gianchandani, 2008)

Thin, perforated aluminum disks are used on both sides of the zeolite disks to improve the temperature uniformity along these surfaces without blocking the gas flow. The assembly is packaged in a thermally insulating polyvinyl chloride (PVC) cavity. The two zeolite disks are peripherally bonded to the cavity using a vacuum grade epoxy to prevent leakage. The common outlet to both sides of the pump is located at the center, and the two inlets are at the top and the bottom of the device. This particular configuration, with a separate zeolite disk pumping gas from either side of a single heater, is termed the double-sided pumping architecture. Also, a singlesided pump, using just one zeolite disk, for example zeolite-1, in Fig. 6.9 is also possible.

In Figure 6.10, a fabricated device can be seen, which has a final packaged volume of 55×55×12 mm^3. It uses two 2.3mm thick, 48mm diameter zeolite disks, and a flexible resistive Kapton heater (18.7 Ω). The heater is a thin, etched-foil resistive element laminated between insulating layers of Kapton.

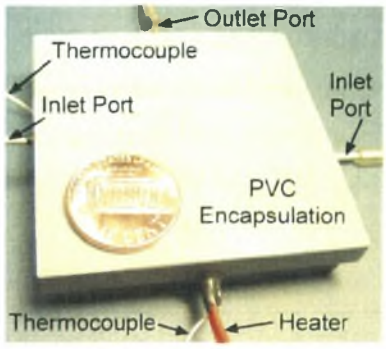

Figure 6.10: Zeolite-based Knudsen pump with PVC encapsulation (Gupta and Gianchandani, 2008)

However, the performance of such a Knudsen pump is constrained by imperfections in clinoptilolite. The equivalent leakage aperture due to imperfections in the natural zeolite samples is estimated by measuring the resistance to isothermal pressure-driven flow. The difference between the measured pressure and the ideal value for the nanoporous material indicates the leakage (Poiseuille) flow as seen in Fig. 6.11. The 1.15 mm thick zeolite samples have typical leak aperture diameters of 10.2–13.5 $\mu m/cm^2$.

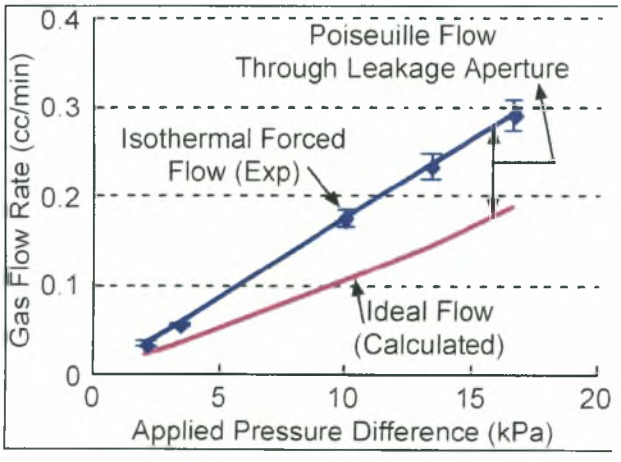

Figure 6.21: Experimental characterization of pressure-driven gas flow across a typical 25mm diameter and 1.15mm thick zeolite disk (Gupta and Gianchandani, 2008)

It appears that a zeolite-based Knudsen pump using naturally occurring nanoporous clinoptilolite, and potentially other zeolites as well, can be built for atmospheric pressure operation. Having no moving parts, it offers the promise of high reliability. The architecture of the Knudsen pump presented by Gupta and

Gianchandani can be potentially extended to serial or parallel multistage pumping. These configurations can result in gas flow rates of 0.005–0.02 cc/min-cm^2 of zeolite disk, or gas pumping pressure on the order of 50 kPa, for power density levels of roughly 1 W/cm^2, and may have potential applications in gas chromatographs, mass spectrometers and systems requiring presice control of gas flow [Gupta & Gianchandani, 2008].

Chapter 7

Concluding remarks

The scope of the present work is to investigate the phenomenon of thermal transpiration, also referred to as "thermal creep". The Knudsen pump, whose "driving principle" is that of thermal transpiration, is particularly suited to miniaturization and fabrication techniques. It has been found that it is an attractive possibility for microscale pumps and macroscale pumps and this attractiveness is attributed to the unique features of Knudsen compressors, such as low power, moderate size, no moving parts and no working fluids.

To this purpose, we apply kinetic model equations in order to investigate the rarefied gas flow through a cylindrical tube, whose ends are maintained at different temperatures.

After a brief introduction and literature review in chapters 1 and 2 respectively, the formulation of the problem is presented in chapter 3. In chapter 4 the numerical scheme is described, while results regarding the flow are presented in chapter 5. In chapter 6, a report on several configurations concerning the Knudsen pump is provided.

The problem is described by the integro – differential Boltzmann equation, which is used to determine the distribution of particles in physical and molecular velocity space, as well as in time. The macroscopic quantities of practical interest are obtained from the moments of the distribution function.

For the modeling of the flow, the ellipsoidal kinetic model and, in particular, the non – linear ellipsoidal model subject to Maxwell diffuse boundary conditions, has been used in the simulations. The numerical solution is based on the discrete velocity method. The results include all macroscopic quantities of practical interest, including the velocity, temperature, heat flux and density in the whole range of the Knudsen number, in terms of the rarefaction parameter δ, the temperature ratio T_{in}/T_{out} and the channel aspect ratio L/R.

In all cases, the axial velocity decreases as the length of the tube increases. As the temperature ratio increases from $T_{in}/T_{out} = 0.1$ to $T_{in}/T_{out} = 0.5$ we can see that the temperature inside the tube increases as well. Also, the axial heat flux is always

positive, denoting, as expected, that heat is moving from the cold side to the hot side of the tube. By applying the streamlines we see that the gas is moving from the cold side (i.e. the right reservoir) to the hot side (i.e. the left reservoir), indicating the presence of the phenomenon of thermal transpiration.

In the future, the implementation of the non linear kinetic equations could be extended to solve problems in more complex geometries, and in a wider range of conditions. A comparison could also be made with some of the already fabricated devices, as well as an estimation of the optimal geometry of a Knudsen pump. A novel concept for the design of innovative Knudsen pumps based on the basic thermal creep theory is a challenging project.

References

1. Aoki, K., Degond, P., Mieussens, L., Nishioka, M. and Takata S., Numerical simulation of a Knudsen pump using the effect of curvature of the channel, *Rarefied Gas Dynamics*, 2007, 1079 – 1084
2. Cardenas, M. R., Graur, I., Perrier, P., and Meolans J. G., *Thermal transpiration flow, 3rd Micro and Nano Flows Conference*, 2011, 1-7
3. Cercignani, *Theory and application of the Boltzmann equation, Scottish Academic Press*, 1975
4. Gad-el Hak, M., *The MEMS Handbook*, CRCPress, Florida, USA, 2002
5. Gupta, N. K., Masters, N. D., Ye, W., and Gianchandani, Y. B., Gas flow in nano – channels: Thermal transpiration models with application to a Si – micromachined Knudsen pump, *Transducers, Solid – state sensors, Actuators and Microsystems*, International Conference, 2007, 2329 – 2332
6. Gupta, N. K. and Gianchandani, Y. B., Thermal transpiration in zeolites: a mechanism for motionless gas pumps, *Applied Physics Letters*, **93**, (19), 2008
7. Han, Y. L., Alexeenko, A., Young, M. And Muntz, E. P., Experimental and computational studies of temperature gradient driven molecular transport in gas flows through nano/micro – scale channels, *Nanoscale and Microscale Thermophysial Engineering*, **11**, (1 – 2), 2007, 151-175
8. Hobson, J. P. and Salzman, D. B., Review of pumping by thermal molecular pressure, *J. Vac. Sci. Technol. A*, **18** (4), 2000, 1758 – 1765
9. Maxwell, J. C., On stress in rarefied gases arising from inequalities of temperature, *Pro. R. Soc. Lond.*, **27**, 1878, 304-308
10. Misdanitis, S., Rarefied gas flow between moving plates with heat transfer, M.Sc. Thesis, Department of Mechanical Engineering, University of Thessaly, Volos, 2009
11. McNamara, S. and Gianchandani, Y. B., A micromachined Knudsen pump for on – chip vacuum, *Transducers, Solid – state sensors,*

Actuators and Microsystems, 12th International Conference, Vol. **2**, 2003, 1919 – 1922

12. Naris, S. and Valougeorgis D., Gas flow in a grooved channel due to pressure and temperature difference, *4th International Conference on Nanochannels, Microchannels and Minichannels*, 2006
13. Pantazis, S., Simulations of transport phenomena in conditions far from thermodynamic equilibrium via kinetic theory with applications in vacuum technology and MEMS, Ph.D. Thesis, Department of Mechanical Engineering, University of Thessaly, Volos, 2011
14. Pharas, K. and McNamara, S., Knudsen pump driven by a thermoelectric material, *Journal of Micromechanics and Microengineering*, **20**, (12), 2010
15. Reynolds, O., On certain dimensional properties of matter in the gaseous state, Part I and Part II, *Philosophical Transactions of the Royal Society of London*, **170**, 28, 1879, 727-845
16. Ritos, K., Lihnaropoulos, Y., Naris, S. and Valougeorgis, D., Pressure- and temperature – driven flows through triangular and trapezoidal microchannels, *Heat Transfer Engineering*, **32** (13-14), 2011, 1101-1107
17. Sharipov, F., Rarefied gas flow through a long tube at any temperature ratio, *J. Vac. Sci. Technol. A*, **14** (4), 1996, 2627 – 2635
18. Sharipov, F., Rarefied gas flow through a long tube at arbitrary pressure and temperature drops, *J. Vac. Sci. Technol. A*, **15** (4), 1997, 2434 – 2436
19. Sharipov, F. M. and Seleznev, V., Data on internal rarefied gas flows, *J. Phys. Chem. Ref. Data*, **27**, 1998, 657–706
20. Sone, Y., A simple demonstration of a rarefied gas flow induced over a plane wall with a temperature gradient, *Phys. Fluids A*, **3** (5), 1991, 997 – 998
21. Sone, Y., Waniguchi, Y. and Aoki, K., One way flow of a rarefied gas induced in a channel with a periodic temperature distribution, *Phys. Fluids*, **8** (8), 1996, 2227
22. Turner, D. J., A mathematical analysis of a thermal transpiration vacuum pump, *Vacuum*, **16**, No. 8, 1966, 413 – 419

23. Vargo, S. E., Muntz, E. P., Shiflett G. R. and Tang W. C., Knudsen compressor as a micro- and macroscale vacuum pump without moving parts or fluids, *J. Vac. Sci. Technol. A*, **17** (4), 1999, 2308 – 2313

24. Young, R. M., Analysis of a micromachine based vacuum pump on a chip actuated by the thermal transpiration effect, *J. Vac. Sci. Technol. B*, 17 (2), 1999, 280 – 287